

May 2024

The Hodgkin-Huxley Model for Neuron Action Potentials: A Computational Study

Uditi Chandrashekhar
Macalester College, uchandra@macalester.edu

Follow this and additional works at: <https://digitalcommons.macalester.edu/mjpa>



Part of the [Physics Commons](#)

Recommended Citation

Chandrashekhar, Uditi (2024) "The Hodgkin-Huxley Model for Neuron Action Potentials: A Computational Study," *Macalester Journal of Physics and Astronomy*: Vol. 12: Iss. 1, Article 4.
Available at: <https://digitalcommons.macalester.edu/mjpa/vol12/iss1/4>

This Honors Project - Open Access is brought to you for free and open access by the Physics and Astronomy Department at DigitalCommons@Macalester College. It has been accepted for inclusion in Macalester Journal of Physics and Astronomy by an authorized editor of DigitalCommons@Macalester College. For more information, please contact scholarpub@macalester.edu.

The Hodgkin-Huxley Model for Neuron Action Potentials: A Computational Study

Abstract

Neurons are the fundamental units of the nervous system that receive stimuli as signals and pass on this information to other cells in different parts of the body. An action potential refers to the transmission of the electrical nerve impulse along the neuron. In their seminal work published in 1952, Alan L. Hodgkin and Andrew Huxley proposed a mathematical model of neuronal membrane action potentials based on a series of experiments they conducted using the giant squid neuron. This thesis is a study of the nature of the action potential used to transfer signals along the neuron based on the Hodgkin-Huxley (HH) model. The model consists of four coupled differential equations that contain non-linear terms and have no analytic solutions, and so numerical methods must be employed. In this work we developed MATLAB programs using the Runge-Kutta and Finite Difference Explicit Method to solve the space-clamped and full spatial and temporal HH equations respectively. Results illustrated that the solutions from these programs are consistent with current understanding of action potential behavior. The space-clamped calculations describe the behavior of an action potential as it evolves through time when a uniform potential is maintained in the neuron. The full spatial and temporal calculations describe how action potentials evolve in both space and time. The results can be interpreted as a type of non-linear diffusion of voltage, but with important differences compared to classical linear diffusion. Finally, some preliminary work on extensions of the HH model is provided.

Cover Page Footnote

I would like to express my deep gratitude to the following people and departments, without whom this project would not have been possible. First and foremost, I would like to thank Professor James R. Doyle for offering the opportunity to work on this project. His guidance, both in the context of research and in general, has set me up for success and I deeply appreciate his commitment to student support. I would like to thank the Macalester Physics and Astronomy Department and all my peers for being a crucial part of the meaningful academic experiences I have had. I would also like to thank my friends, professors in the Psychology and Educational Studies Departments, and the International Student Programs Department. Last but not least, my immense gratitude to my family for supporting my educational endeavors.

Advisor: James R. Doyle

Department of Physics and Astronomy

Macalester College

April 29, 2024

“All models are wrong, but some are useful.”

George E. P. Box

Chapter I: Introduction

A. Neurons and Action Potentials

Neurons are specialized, excitable cells that are the fundamental units of the nervous system. In human beings, billions of neurons form a dense network to receive stimuli as signals and pass on this information to other cells in different parts of the body. The human brain itself contains approximately 100 billion (10^{11}) neurons [1]. The structure of a typical neuron is shown in Figure 1.1. The four main parts of the simplest model of the neuron are the cell body, dendrites, axon, and branching terminal. The connections between neurons are known as synapses, where chemicals called neurotransmitters are used to pass signals from one cell to the other [2]. There are about 100 trillion (10^{14}) synapse connections in the human brain [3]. Dendrites are connected via synapses to other neurons as shown in Figure 1.1. The cell body contains the cell nucleus and has a long extension known as the axon. The axon is the part of the neuron responsible for conducting nerve impulses that are electrical in nature and is often surrounded by a myelin sheath. The axon ends in the presynaptic terminal. Dendrites receive neurotransmitters from other neurons, and if the total stimulus is above a certain threshold, an electrical pulse known as an action potential is generated at the axon hillock that propagates down the axon. When the action potential reaches the presynaptic terminal, neurotransmitters are released and absorbed by the dendrites of the other neurons, and the transmission process continues [4].

Neurons come in many different forms categorized by the different roles they play such as sensory neurons, motor neurons, and interneurons. In comparison to other cells, neurons have the unique ability to modify structure and/or function depending on the nature of stimuli from their environment. This feature of neurons is known as neuronal plasticity and allows learning and other adaptations to occur [5].

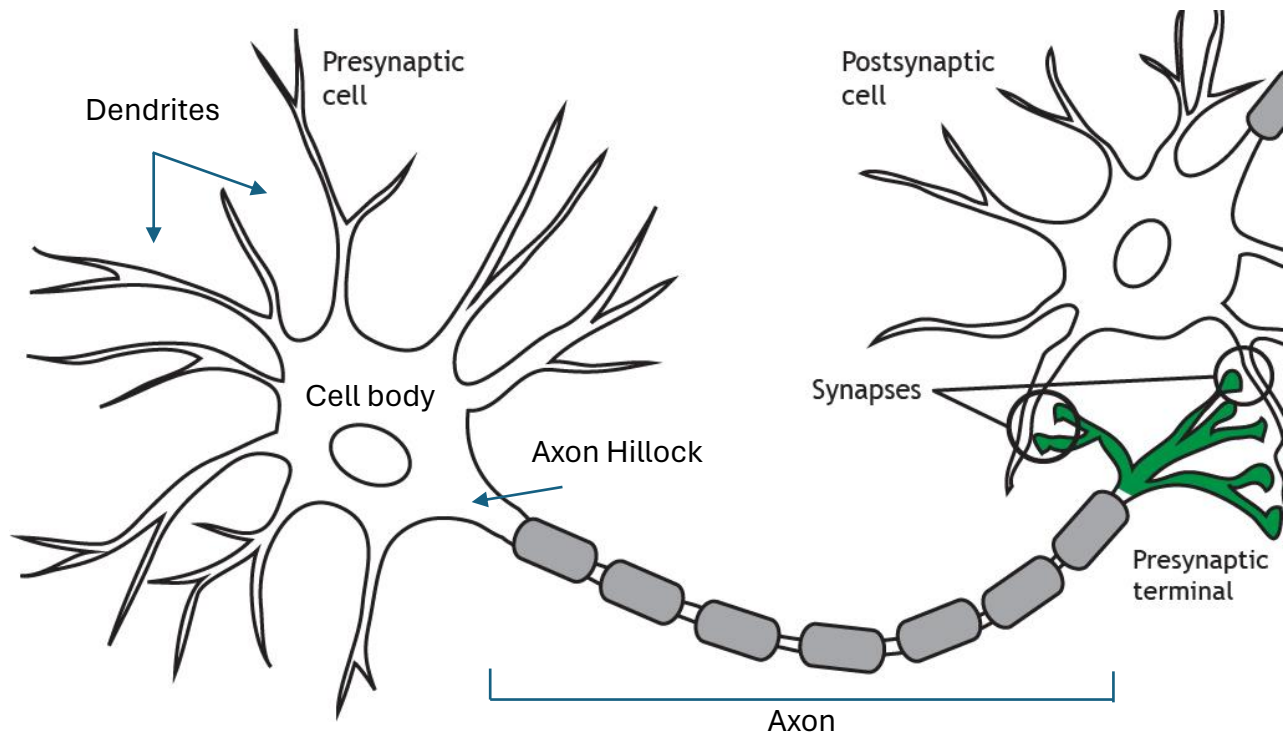


Figure 1.1. Labelled diagram of the structure of the neuron with synapses. Adapted from 'Presynaptic Terminal' by [Casey Henley](#) licensed under a [Creative Commons Attribution Non-Commercial Share-Alike \(CC-BY-NC-SA\) 4.0 International License](#) [6]

B. Background for Mathematical Model of Action Potentials

In their seminal work published in 1952, Alan L. Hodgkin and Andrew Huxley proposed a mathematical model of neuronal membrane action potentials based on a series of experiments they conducted using the giant squid axon. Given that giant squid axons can be as long as one meter with a diameter of one millimeter, Hodgkin and Huxley were able to use a voltage-clamp technique to measure the membrane potential in the axon. In this technique the membrane potential is maintained at a fixed value while input and output currents are measured. Through their observations and results they constructed a mathematical model of the cell membrane comprising elements of an electrical circuit [7]. This work earned Hodgkin and Huxley the Nobel Prize in Physiology or Medicine in 1963.

This thesis is a study of the nature of the action potential used to transfer signals along the axon based on the Hodgkin-Huxley (HH) model. The remainder of this chapter will provide some necessary background information on potentials across membranes, specifically the derivation of the equilibrium or resting membrane potential. This will be followed by a qualitative description of the formation of the action potential which represents a deviation from this resting potential. Subsequent chapters will discuss the details and computational implementation of the HH model.

1. Membrane Potential and Ion Transport

Propagation of electrical impulses in the axon is possible when there is a potential difference between the interior and the exterior of the neuron across the cell membrane that is different than the equilibrium potential difference. In the case of cells in the human body, differences in ionic concentrations inside and outside the cell membrane create the membrane potential difference,

known as the membrane potential. Movement of ions is facilitated either by ion channels composed of membrane bound proteins that use either active or passive transport mechanisms since all cell membranes are composed of lipids that are impermeable to ions. Active transport means that energy is required to move ions and is present in neurons in the form of sodium/potassium pumps that reestablish the equilibrium potential in the membrane once an action potential has passed. The molecule ATP supplies this energy. Passive transport includes voltage-gated channels and non-gated channels that are always open. These do not require energy input [8].

When the cell is at rest and there is no net transport movement of ions, the resulting membrane potential value is referred to as the resting potential. The most relevant ions for membrane potential formation are sodium (Na^+), potassium (K^+) and chlorine (Cl^-). In the resting condition, the concentration of K^+ ions is higher inside the cell and the concentrations of Na^+ and Cl^- are higher outside the cell. When Na^+ ions enter the cell, the neuron is said to be depolarized whereas when Cl^- ions enter, or K^+ ions leave the cell, the neuron is said to be hyperpolarized. As we will see in Chapter 2, depolarization of the neuron followed by hyperpolarization is what constitutes the action potential.

The resting or equilibrium membrane potential is a result of a balance between chemical potential driving forces due to differences in ionic concentrations between the inside and outside of the cell, and the electrical driving forces caused by the separation of ions. For example, if we consider the K^+ ions by themselves, if there is a greater concentration of K^+ ions inside the cell than outside, a chemical potential difference drives the movement of K^+ ions out of the membrane towards an equalized concentration. However, the movement of positive ions out of the neuron results in a potential difference which inhibits further transfer of ions. Eventually an

equilibrium is reached where the diffusive driving force and the potential difference driving force balance. The Nernst or equilibrium potential refers to the membrane potential when equilibrium of a specific ion is achieved.

2. The Nernst Potential

In this subsection the Nernst potential equation, which can be applied to one ion at a time, will be derived. The actual membrane potential depends on K^+ , Na^+ and Cl^- ions, and its value can be calculated using the Goldman-Hodgkin-Katz (GHK) equation that represents an extension of the Nernst equation.

In what follows, $[C](x)$ refers to the concentration of one ionic species and $V(x)$ refers to the potential difference at the spatial point x in the membrane.

As stated earlier, the movement of ions will have a diffusive aspect associated with the difference in concentration of ions inside and outside the cell. Electrostatic forces develop because of the charge separation as the ions diffuse across the membrane through ion channels. The nature of the diffusive forces is illustrated by Fick's law of diffusion.

$$F_{diff} = -D \frac{\partial [C](x)}{\partial x} \quad (1.1)$$

where F_{diff} is the diffusive flux in $cm^{-2}s^{-1}$. The units of the diffusion constant D are cm^2/s . In general, the value of the diffusion constant is dependent on the medium of diffusion and the size of the ion. As an approximation for K^+ , Na^+ and Cl^- ions that we are interested in, the typical value around $D = 3 \times 10^{-6} \frac{cm^2}{s}$ [9].

The transport due to electrostatic forces can be described by the microscopic version of Ohm's law resulting in the drift flux F_{drift} :

$$F_{\text{drift}} = -\mu z[C](x) \frac{\partial V(x)}{\partial x} \quad (1.2)$$

where μ is the mobility with units $\text{cm}^2/\text{V}\cdot\text{s}$. The parameter z refers to the valence of the ion. The partial derivative is just the expression for the electric field with units of V/cm .

At rest the diffusive and the drift fluxes are equal. In addition, Einstein's relation between the diffusion constant and the mobility can be used to eliminate the diffusion coefficient [10]:

$$D = \frac{k_B T}{q} \mu = \frac{RT}{F} \mu \quad (1.3)$$

where, k_B refers to the Boltzmann's constant with units of J/K , T refers to the absolute temperature in Kelvin, and q is charge of the ion in units of Coulombs. Combining equations 1.1, 1.2 and 1.3 the following equations we find for the net ion flux:

$$F_{\text{total}} = F_{\text{diff}} + F_{\text{drift}} \quad (1.4)$$

$$F_{\text{total}} = -D \frac{\partial [C](x)}{\partial x} - \mu z [C](x) \frac{\partial V(x)}{\partial x} \quad (1.5)$$

$$F_{\text{total}} = -\frac{k_B T \mu}{q} \frac{\partial [C](x)}{\partial x} - \mu z [C](x) \frac{\partial V(x)}{\partial x} \quad (1.6)$$

If we multiply F_{total} by the ion valence z and use the relations $k_B = \frac{R}{N_A}$ where R is the ideal gas constant and N_A is Avogadro's number, and the Faraday constant $F = q N_A$ we can derive the Nernst-Planck equation below:

$$J_{\text{total}} = -\left(\frac{\mu}{N_A} z R T \frac{\partial [C](x)}{\partial x} + \frac{\mu}{N_A} z^2 F [C] \frac{\partial V(x)}{\partial x} \right) \quad (1.7)$$

where, J_{total} , refers to the current density with units of A/cm^2 .

Setting equation 1.7 equal to 0 will allow us to derive an expression for the Nernst equation, which represents the equilibrium potential difference across the membrane:

$$J_{total} = -\left(\frac{\mu}{N_A} zRT \frac{\partial[C](x)}{\partial x} + \frac{\mu}{N_A} z^2 F [C](x) \frac{\partial V(x)}{\partial x}\right) = 0 \quad (1.8)$$

$$\frac{\partial V(x)}{\partial x} = -\left(\frac{N_A}{\mu z^2 F [C](x)}\right) \left(\frac{\mu}{N_A} zRT \frac{\partial[C](x)}{\partial x}\right) \quad (1.9)$$

with the solution

$$V_{eq} = V_{in} - V_{out} = -\frac{RT}{zF} \ln \frac{[C]_{in}}{[C]_{out}} \quad (1.10)$$

The Nernst equation is an expression for the potential difference for a single ionic species. For an actual membrane, the equilibrium (or resting) potential will require the net current due to all ions present is equal to 0. Assuming that the three main ions for a neuronal membrane are K^+ , Na^+ and Cl^- and that they move independently, using a similar approach to the Nernst potential derivation above leads to a generalized equation known as the Goldman-Hodgkin-Katz (GHK) equation which can be used to calculate the resting potential [8]:

$$V_M = \frac{RT}{F} \ln \left(\frac{P_K [K^+]_{out} + P_{Na} [Na^+]_{out} + P_{Cl} [Cl^-]_{out}}{P_K [K^+]_{in} + P_{Na} [Na^+]_{in} + P_{Cl} [Cl^-]_{in}} \right) \quad (1.11)$$

where the parameters, P_K , P_{Na} and P_{Cl} , refer to the permeabilities of the ionic species.

In this paper the focus will be on values that are specific to the squid neuron, the case considered in the original Hodgkin Huxley work. The ionic permeabilities are in the ratio $P_{K^+} : P_{Na^+} : P_{Cl^-}$ as 1: 0.03: 0.1 and Table 1.1 provides the relevant values of the concentrations [11]. At $T = 20^\circ C$ we find from Equation 1.11 that the equilibrium potential difference is -74 mV, close to the

equilibrium Nernst potential for K^+ . This result is not surprising given the high relative permeability of K^+ compared to Na^+ and Cl^- given above.

Table 1.1 Ion concentrations in squid neuron (from Johnston and Wu, 1995 [11])

Ion	Inside concentration (mM)	Outside concentration (mM)	Equilibrium potential (mV) $T = 20\text{ }^\circ\text{C}$
K^+	400	20	$58 \ln \frac{20}{400} = -75$
Na^+	50	440	$58 \ln \frac{440}{50} = +55$
Cl^-	40~150	560	$-58 \ln \frac{560}{40\sim 150} = -66 \text{ to } -33$

3. Qualitative Description of the Action Potential

An action potential refers to the transmission of the electrical nerve impulse along the axon. The action potential thus represents a deviation in space and time from the equilibrium potential described by Equation 1.11. The crucial concept needed here is that of voltage-gated ion channels. These are proteins embedded in the lipid bilayer whose permeability is sensitive to the membrane potential and are opened when the membrane potential sufficiently deviates from the equilibrium potential. Note that the concentration of Na^+ ions outside the cell is much larger than inside the cell, while the reverse is true for K^+ ions (Table 1). When a sufficiently large depolarization occurs in the axon hillock (see Figure 1.1) due to the action of neurotransmitters in the cell body received through the dendrites, voltage-gated ion channels are opened to allow excess Na^+ ions to enter the cell, further depolarizing the cell. The result is a rapid increase in the membrane potential which approaches zero from the equilibrium value of -74 mV.

At some value of the membrane potential the Na^+ voltage-gated channels begin to close and the K^+ voltage gated channels open, with the result that the flux of Na^+ ions into the cell stops and K^+ ions (in large concentration inside the cell) begin flowing out of the cell. Thus, the inside of the cell loses positive ions, and the membrane potential begins to decrease back towards the equilibrium potential. When the potential reaches the equilibrium potential, the K^+ channels are not completely closed, so that the potential overshoots the equilibrium potential, giving rise to the refractory period. An important property of the refractory period is that the Na^+ channels are not only closed but are also in an inactive state, so that another action potential cannot be initiated during this time at this location. Another consequence of the inactive Na^+ channels is that only Na^+ channels downstream that have not yet experienced an action potential can generate a new action potential. This has the effect of the action potential propagates in only one direction down the axon. Eventually, after the action potential has passed a given point, active sodium-potassium pump proteins in the membrane fueled by ATP re-establish the equilibrium concentrations of the Na^+ and K^+ ions.

Further details on the mechanism, along with their mathematical implementation, will be discussed in Chapter 2.

C. Thesis Outline and Goals

The processes outlined above can be modeled using the equations proposed by Hodgkin and Huxley in their seminal 1952 paper (HH 1952). The model consists of four coupled differential equations: one partial differential equation that describes the temporal and spatial variation of the membrane potential, and three ordinary differential equations that represent the dynamics of

the voltage gated ion channels. These equations contain non-linear terms and have no analytic solutions, and so numerical methods must be employed. It is worth noting that there are other models that have been inspired by the HH equations, such as the Morris-Lecar equations, and the FitzHugh-Nagumo equations. They are simplified versions of the HH model and the Fitz-Hugh-Nagumo equations in particular are often used to study excitability of neurons [8, 12]. However, the focus of this thesis is exploring the generation and propagation of action potentials using the original HH model.

The goals of this thesis include development of algorithms using standard numerical methods to calculate HH action potentials, to verify that the solutions are consistent with the current understanding of action potential formation and propagation, and to provide a foundation for further applications such as addition of stochastic phenomena into the theory. Chapter 2 will provide an overview of the HH model and develop the space-clamped equations. Chapter 3 will focus on the results of the space-clamped calculations that describe the behavior of an action potential as it evolves through time when a uniform potential is maintained in the axon. Chapter 4 will focus on the more challenging problem of how action potentials evolve in both space and time. Finally, Chapter 5 will discuss some preliminary work further extensions of the HH model, for example the inclusion of stochastic effects.

Chapter II: Space-Clamped HH Equations

A. Introduction

Chapter 1 described how the movement of ions across the membrane determines the electrical properties of neurons and that the flow of current is dependent on the permeabilities of the neuron membrane to relevant ionic species. It was also claimed that for an action potential to be propagated along the axon, a sufficiently large depolarization must occur in the axon hillock (see Figure 1.1). The GHK equation (Equation 1.11) is specific to the resting condition and does not account for changes in permeabilities that are needed for membrane action potentials. It is the change in permeability of the membrane to Na^+ ions that causes the initial depolarization of the membrane potential to start an action potential and thus there is the need for a model that goes beyond the equilibrium GHK equation [8].

1. Electrical Circuit Model

A very useful model to describe the behavior of the action potential is the equivalent electrical circuit model, proposed and verified experimentally by Hodgkin and Huxley. In this model the impermeable membrane is represented by a capacitor, the ion channels by voltage dependent resistors, and the ion concentration gradients as voltage sources (see Figure 2.1) [7].

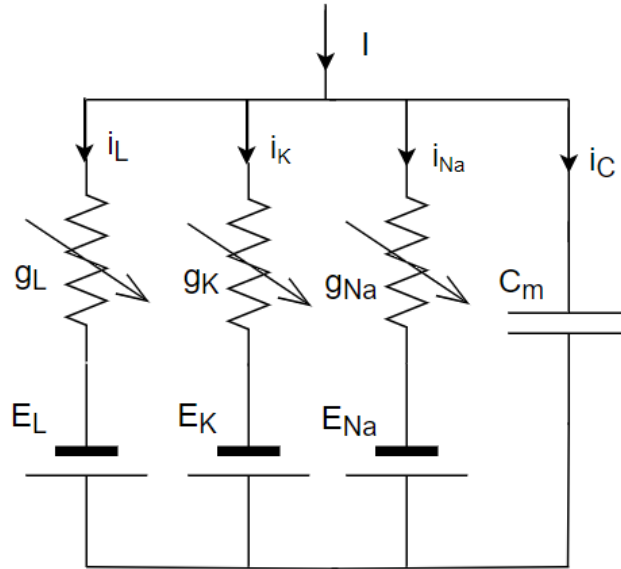


Figure 2.1. Equivalent Electrical Circuit Model

where, E_{Na} , E_K , and E_L refers to the Nernst potential of ionic species Na^+ , K^+ and leak mainly comprising Cl^- ions, g_{Na} , g_K , and g_L denote their respective conductance per unit area, ($mmho/cm^2$) and C_M refers to membrane capacitance per unit area ($\mu F/cm^2$) [7]. An external current I is included to account for the experimental conditions as discussed below.

In the mathematical analysis conducted by Hodgkin and Huxley (1952) [7] the total current in the circuit was divided into a capacitance current and an ionic current. Recall, that for a capacitor:

$$Q = C_M V_M \tag{2.1}$$

$$i_{cap} = \frac{dQ}{dt} = C_M \frac{dV_M}{dt} \tag{2.2}$$

where, Q refers to charge on the capacitor in Coulombs, V_M is the potential difference across the membrane in mV, and t refers to time in milliseconds. i_{cap} is the total capacitance current per unit area in the circuit.

We can build up an understanding of this model by focusing first on a membrane that is only permeable to one ionic species, Na^+ for instance in Figure 2.2.

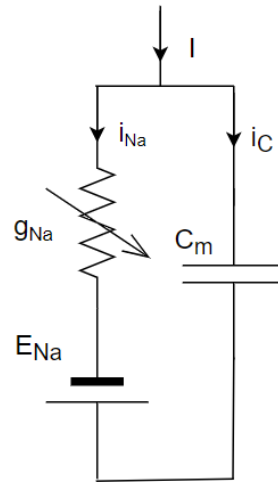


Figure 2.2. Equivalent electrical circuit for one ionic species, sodium

If we denote \hat{g}_{Na} as the conductance of a single Na^+ channel, and the Nernst potential as E_{Na} we can apply Ohm's law and find the expression for the ionic current per channel:

$$\hat{i}_{Na} = \hat{g}_{Na}(V_M - E_{Na}) \quad (2.3)$$

Supposing there are N_{Na} number of Na^+ channels in a given unit area of the membrane, we see that the circuit in Figure 2.2 is represented where $g_{Na} = N_{Na} \times \hat{g}_{Na} = \frac{1}{r_{Na}}$. Thus, the current per unit area can be written as:

$$i_{Na} = g_{Na}(V_M - E_{Na}) = \frac{V_M - E_{Na}}{r_{Na}} \quad (2.4)$$

Applying Kirchoff's node rule to the circuit in Figure 2.2, we see that the capacitance current per unit area and the ionic current from sodium channels must equal to the external current I :

$$i_{cap} + i_{Na} = I \quad (2.5)$$

$$C_M \frac{dV_M}{dt} + \frac{V_M - E_{Na}}{r_{Na}} = I \quad (2.6)$$

$$C_M \frac{dV_M}{dt} = -\frac{V_M - E_{Na}}{r_{Na}} + I = -g_{Na}(V_M - E_{Na}) + I \quad (2.7)$$

This approach can be easily extended to include to the other ionic species, giving the following expression that characterizes the circuit shown in Figure 2.1:

$$C_M \frac{dV_M}{dt} = -g_K(V_M - E_K) - g_{Na}(V_M - E_{Na}) - g_L(V_M - E_L) + I \quad (2.8)$$

2. Conductance Values and Voltage Dependence

As voltage-gated ion channels, the conductance of the Na^+ and K^+ channels will vary with membrane potential. Hodgkin and Huxley found empirically that for the potassium conductance the following relation provided a best fit to their experimental results:

$$g_K = n^4 \bar{g}_K \quad (2.9)$$

where the opening and closing of the channel is governed by the rate equation

$$\frac{dn}{dt} = \alpha_n(1 - n) - \beta_n n \quad (2.10)$$

In this expression \bar{g}_K refers to a constant maximum value of the conductance per unit area for potassium channels, n refers to a dimensionless variable that takes on values between 0 and 1. and α_n and β_n are voltage dependent rate constants having units of msec^{-1} .

The physical interpretation of these equations is as follows. For K^+ ions to cross the neuron membrane there are four identical components of the channel that must be activated. n represents the probability that a given component is activated, and the probability that all four channels are open is thus n^4 . Equation 2.10 is a rate equation for n where the first term represents the rate at which a component is open, and the second term represents the rate at which it closes.

A similar set of equations is proposed for Na^+ ions:

$$g_{Na} = m^3 h \bar{g}_{Na} \quad (2.11)$$

$$\frac{dm}{dt} = \alpha_m(1 - m) - \beta_m m \quad (2.12)$$

$$\frac{dh}{dt} = \alpha_h(1 - h) - \beta_h h \quad (2.13)$$

where, \bar{g}_{Na} refers to a constant maximum value of the conductance per unit area for sodium channels, n and h refer to dimensionless variables that takes on values between 0 and 1. Again the α and β rate constants are dependent on voltage but not time.

The interpretation for the variable m is similar to the explanation provided for n in potassium channels. There are 3 components to the gate that must be activated to allow ion transfer. In addition, the h variable corresponds to an inactivating component. The presence of both activating and inactivating components for the Na^+ channels is essential to the nature and behavior of the action potential. As mentioned in Chapter 1, inactivation of the Na^+ channel is

responsible for refractory period and results in unidirectional transport of the action potential

Figure 2.3 shows a schematic picture of the Na^+ channel.

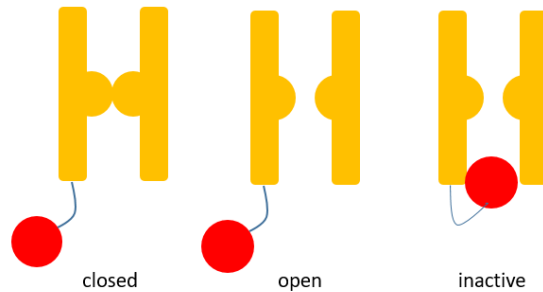


Figure 2.3. Model for the activating and inactivating molecules for sodium

This model is known as the ball and chain model. When a minimum potential difference is present the three components of the gate will be activated the gate will open. With a higher voltage the inactivating component, represented by the ball locks the channel, giving the refractory period of an action potential. During the refractory period, a new action potential cannot be generated. Eventually the ball is released from the channel and the channel closes, ready for the next action potential. Figure 2.4 illustrates the main processes in the action potential.

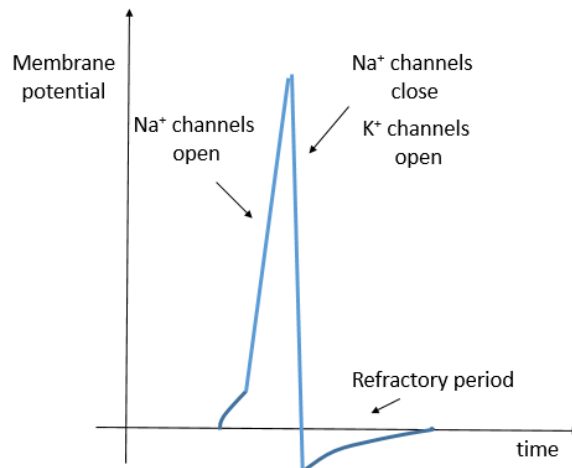


Figure 2.4. Processes of the action potential

Expressions for the rate constants where α_i and β_i were deduced by Hodgkin and Huxley based on experimental data from the squid axon:

$$\alpha_n(V) = \frac{0.01(V + 10)}{\exp\left(\frac{V + 10}{10}\right) - 1} \text{ msec}^{-1}$$

$$\beta_n(V) = 0.125 \exp\left(\frac{V}{80}\right) \text{ msec}^{-1}$$

$$\alpha_m(V) = \frac{0.1(V + 25)}{\exp\left(\frac{V + 25}{10}\right) - 1} \text{ msec}^{-1}$$

$$\beta_m(V) = 4 \exp\left(\frac{V}{18}\right) \text{ msec}^{-1}$$

$$\alpha_h(V) = 0.07 \exp\left(\frac{V}{20}\right) \text{ msec}^{-1}$$

$$\beta_h(V) = \frac{1}{\exp\left(\frac{V + 30}{10}\right) + 1} \text{ msec}^{-1}$$

Although the form of these equations are empirical fits to experimental results, subsequent work has proposed more physical motivations based on activation energy and thermodynamic considerations [12].

The set of equations 2.8 through 2.13 are known as the space-clamped version of the HH equations. The equations describe a non-propagating action potential in which a uniform voltage along the axon is experimentally maintained and no propagation in space occurs. In Chapter 4 we will discuss modifications to this model to include spatial effects.

B. Numerical Implementation

In this section we describe the numerical methods used to solve the space-clamped HH equations. The simplest procedure is known as the Euler method [13]. Given the initial value problem:

$$\frac{dV}{dt} = f(V, t) \quad V(t = 0) = V_0$$

the idea is that we divide the total time interval T into N divisions of length $\Delta t = h$. That is, we have times $t_0 = 0$, $t_1 = h$, $t_2 = 2h$, etc. We then approximate the value of $V(t_{i+1})$

$$V(t_{i+1}) = V(t_i) + hf(V(t_i), t_i)$$

The Euler method is very simple to implement, but very small values of h (and hence very large values of N) are needed to produce an accurate result. More precisely, the local truncation error is $O(h^2)$ and the total accumulated error is $O(h)$ [13]. The Euler method is seldom used for high precision calculations. Our interest in the method is that it lends itself easily to the introduction of stochastic terms in the HH equation (the Euler-Maruyama method). This will be discussed further in Chapter 5.

More commonly, a version of the Runge-Kutta method is used to integrate initial value differential equations, with the 4th order method the most popular [14]. In the Euler method, one uses the slope of the line at t_i to estimate the value of V at t_i+h . In Runge-Kutta methods, slopes are calculated using the midpoint between t_i and t_i+h as well as the endpoint $t_i + h$, then averaged to estimate a more accurate value of V at $t_i + h$. The equations for the 4th order method are [14]

$$k_1 = hf(t_i, V_i)$$

$$k_2 = hf \left(t_i + \frac{1}{2}h, V_i + \frac{1}{2}k_1 \right)$$

$$k_3 = hf \left(t_i + \frac{1}{2}h, V_i + \frac{1}{2}k_2 \right)$$

$$k_4 = hf(t_i + h, V_i + k_3)$$

$$V_{i+1} = V_i + \frac{1}{6}k_1 + \frac{1}{3}k_2 + \frac{1}{6}k_4 + O(h^5)$$

which has a local truncation error of $O(h^5)$. The total accumulated error is $O(h^4)$, and thus the accuracy of the calculation increases much faster with decreasing h as compared to the Euler method [13]. Even more efficient calculations can be obtained using so-called adaptive Runge-Kutta methods, where the error is estimated at each point and the step size is adjusted accordingly.

In the presentation of space-clamped results in Chapter 3, the 4th order Runge-Kutta method (without adaptation) will be used exclusively. The accuracy of the results will be estimated empirically by considering key results as a function of decreasing step size.

Chapter III. Space-Clamped Results

A. Introduction

In this chapter, the results of the space-clamped calculations using the Runge-Kutta (RK) method will be presented. The equations were programmed in MATLAB. Regardless of the specific model used, two important features of the action potential are the “all-or-nothing” behavior and the presence of a refractory period. The all-or-nothing behavior refers to the sensitivity to a minimum threshold input, below which no action potential is generated. Above the threshold the action potential fires to its full value. No partial action potentials are generated. The refractory period refers to the time period after the depolarization of the neuron where no new action potential can be generated even with above-threshold stimulus [15]. The refractory period arises because of the presence of both activating and inactivating components of the Na^+ ion channels as discussed in Chapter 2 [7].

In the original set of papers by Hodgkin and Huxley, action potentials in the squid neuron were studied using the voltage-clamped technique where the internal potential is maintained at a fixed value with input and output currents being controlled and measured respectively [7]. In our MATLAB programs the resting potential was taken as 0 mV with all other voltages expressed relative to that value. The main variable that was studied were threshold values of the input current. Both currents and voltages can be used to initiate an action potential. The two methods are related, in that a stimulus current will charge up the membrane capacitance and produce a membrane potential that deviates from equilibrium. In the original HH work (and most subsequent work) current initiation was used and we will follow that practice there.

In numerical calculations choosing an appropriate time step is crucial in ensuring that the resolution of the results is sufficient at the end of the chapter the dependence of the results on the choice of time step will be considered.

B. Results

1. Below Threshold Current

The threshold current (to three significant figures) for initiating an action potential was found to be $2.24 \frac{\mu\text{A}}{\text{cm}^2}$. When the input current per area is below threshold, an action potential does not fire. Figure 3.1 shows the result for a subthreshold current $i_{input} = 1.00 \frac{\mu\text{A}}{\text{cm}^2}$. There is a mild disturbance to the membrane potential but no significant deviation from the resting potential (see Figure 3.1).

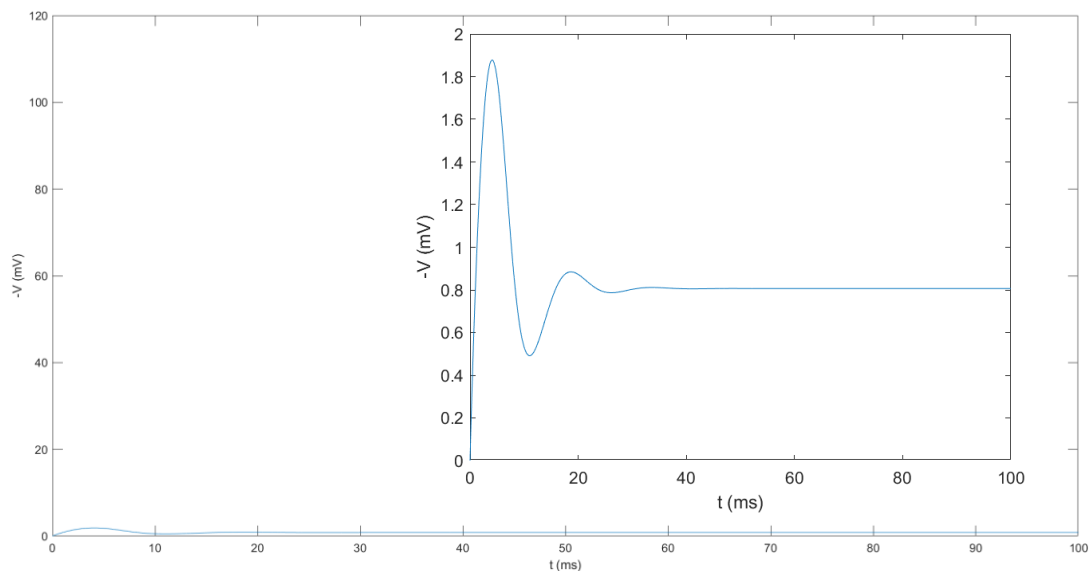
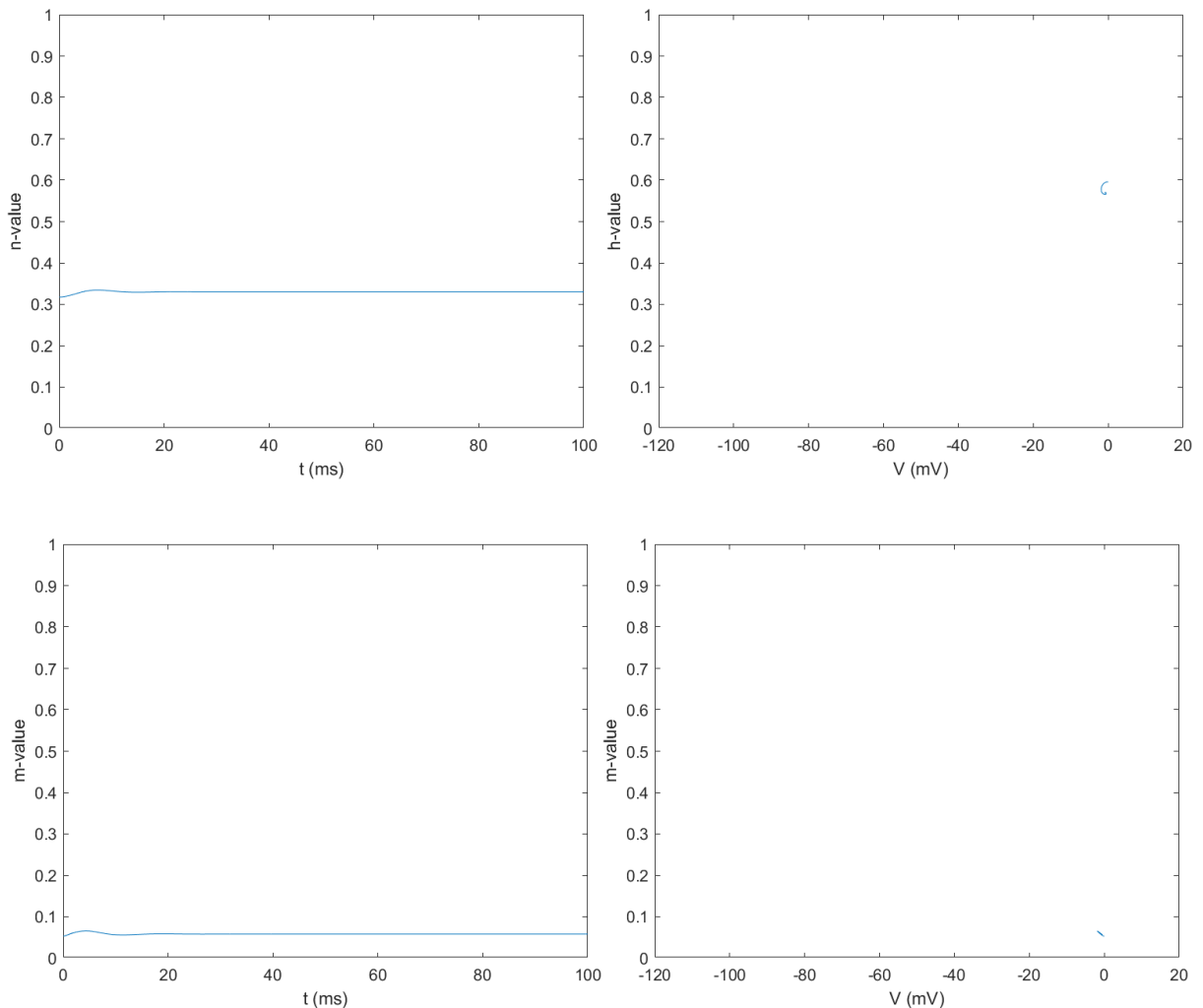


Figure 3.1. Below threshold input current effect on voltage as a function of time. at $i_{input} =$

$1.00 \frac{\mu\text{A}}{\text{cm}^2}$. There is only a slight disturbance from the resting value as is seen in the magnified

picture.

It is of interest to examine the behavior of $n(t)$, $m(t)$, and $h(t)$ as well as $V_M(t)$. In addition, since the HH are non-linear due to the voltage dependences in the α_i and β_i rate constants, phase space plots of the gating variables (n , m , and h versus V) are usually considered. Phase space plots can provide information about the system dynamics that may not be apparent from the time plots. For example, characteristics such as limit cycles and chaotic behavior are often manifested in phase space. Figure 3.2 gives the $n(t)$, $m(t)$, and $h(t)$ and the corresponding phase plots for subthreshold currents.



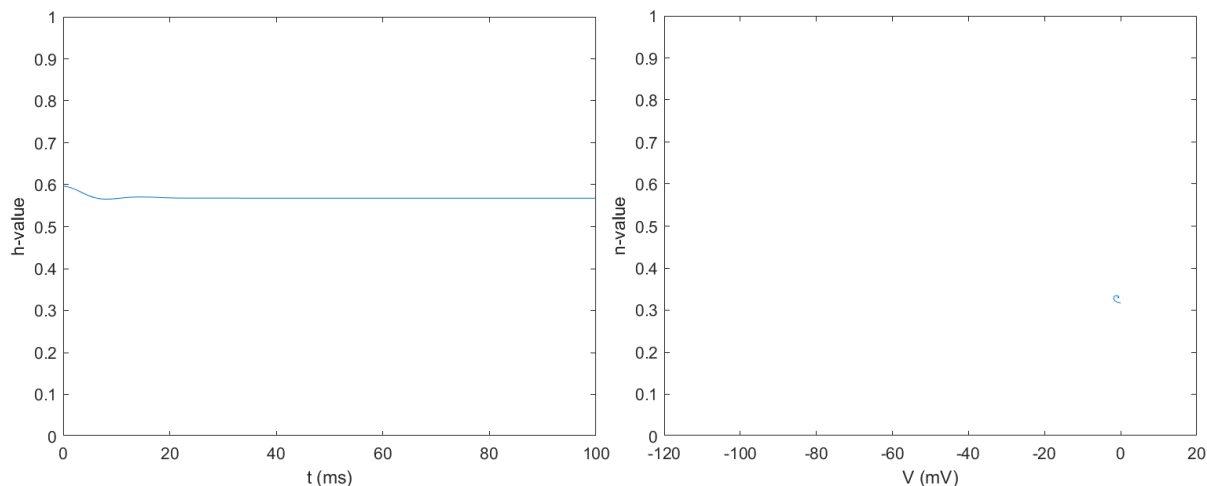


Figure 3.2. Gating variables vs. time and voltage at pre-threshold $i_{input} = 1.00 \frac{\mu\text{A}}{\text{cm}^2}$

2. Single Action Potential

A single action potential can be generated with a current at the threshold $i_{input} = 2.24 \frac{\mu\text{A}}{\text{cm}^2}$. It is noteworthy to observe that after firing the voltage does not go back to resting potential but a value slightly higher (see Figure 3.3). The gating variables cycle from their starting point in the phase plots in a well-defined path (see Figure 3.4), illustrating the depolarization and hyperpolarization of the cell membrane during the action potential.

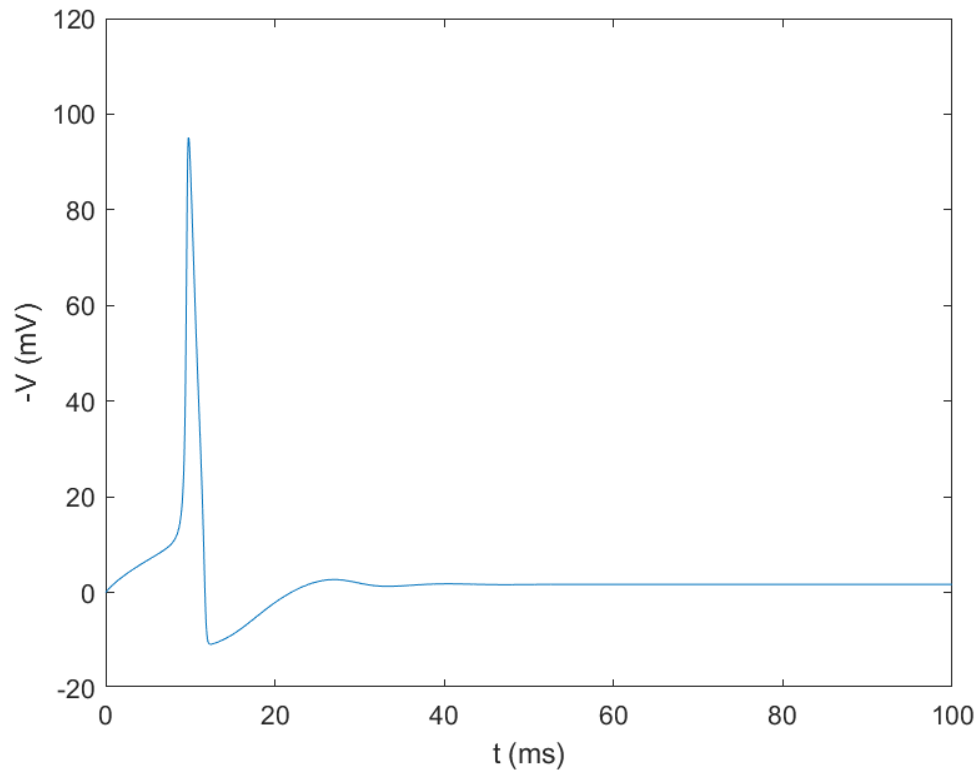
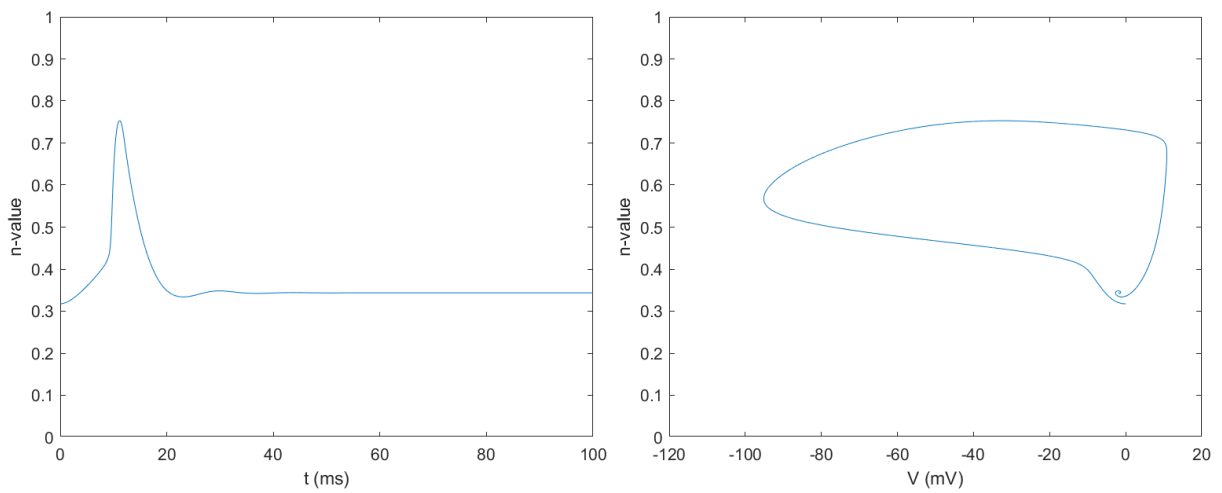


Figure 3.3. Single Action Potential for $i_{input} = 2.24 \frac{\mu A}{cm^2}$



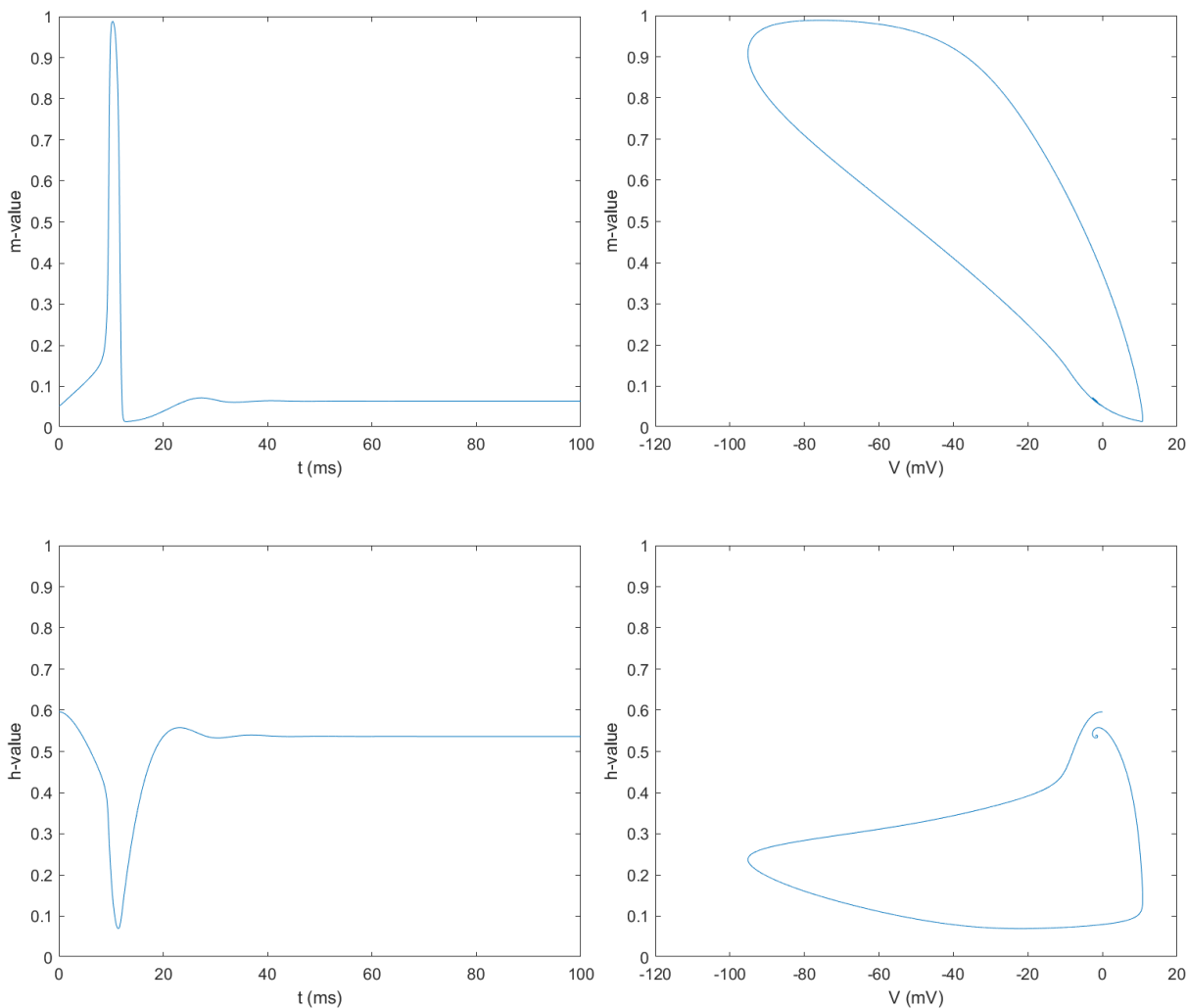


Figure 3.4. Gating variables vs. time and voltage at pre-threshold $i_{input} = 2.23 \frac{\mu A}{cm^2}$

We note that the current threshold for the action potential initiation is very precise. A current of $2.23 \frac{\mu A}{cm^2}$ will not generate an action potential, but rather behavior similar to that in Figures 3.1 and 3.2. (to three significant figures the threshold current is $2.239 \frac{\mu A}{cm^2}$, and no action potential is generated for $i = 2.238 \frac{\mu A}{cm^2}$, – see Chapter 5). This illustrates the “all or nothing” characteristic of the action potential and is due to the non-linearity of the equations. Also note that the

inactivating variable h does not quite return to its starting value after the action potential subsides for a long period of time.

3. Multiple Action Potentials

At a higher currents that exceed the threshold for a single action potential repeated action potentials can be generated, allowing for the expected refractory period. As the excitation current is increased beyond the threshold for generating a single action potential, ripples can be observed in the membrane potential after the refractory period. As the current approaches the threshold for repeated action potentials these perturbations grow (see Figure 3.5). At the minimum threshold for multiple action potentials of $5.97 \frac{\mu\text{A}}{\text{cm}^2}$, two peaks are observed, with the second one being slightly lower in magnitude to the first peak (see Figure 3.6).

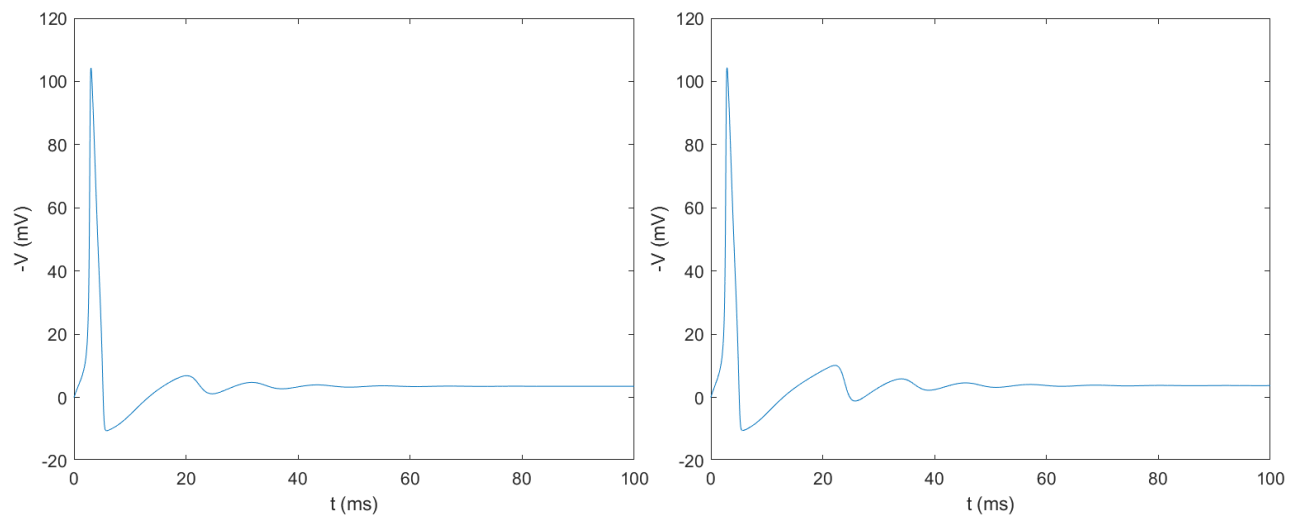


Figure 3.5. Action potentials for $i_{input} = 5.50 \frac{\mu\text{A}}{\text{cm}^2}$ and $i_{input} = 5.96 \frac{\mu\text{A}}{\text{cm}^2}$

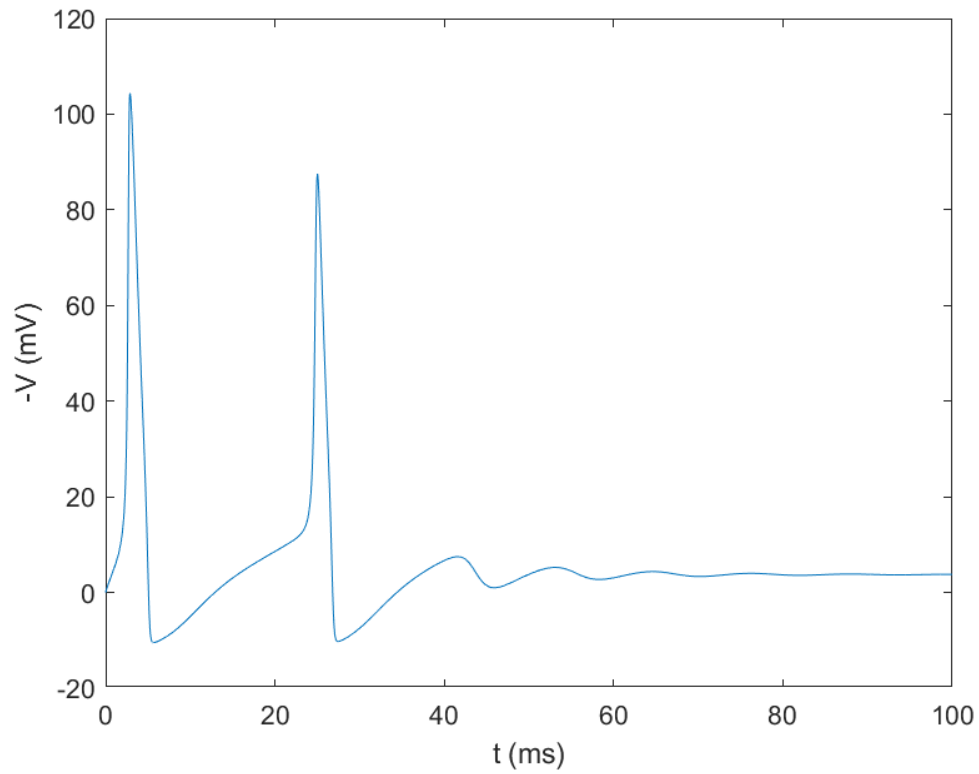
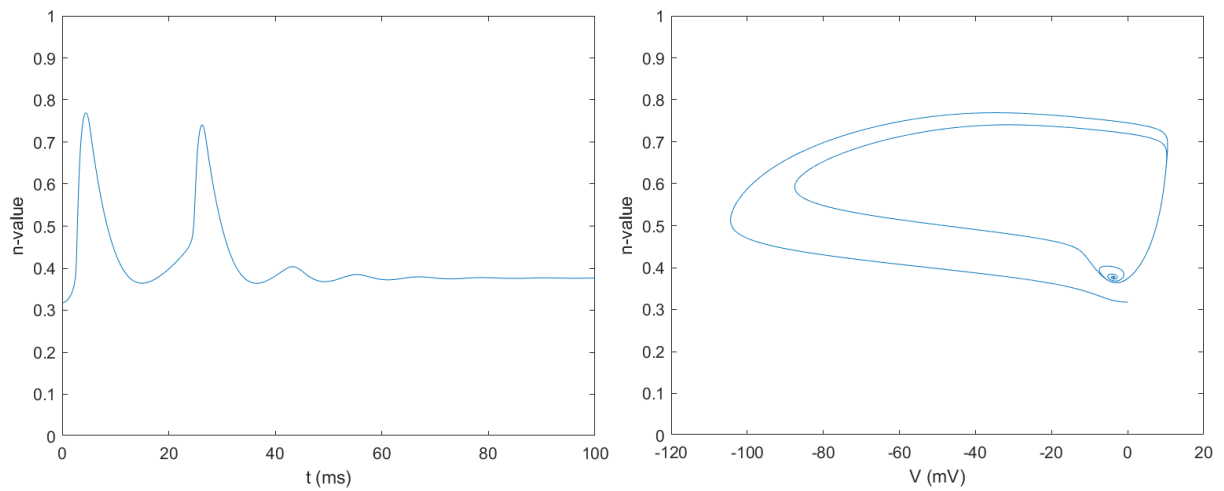


Figure 3.6. Action potential for $i_{input} = 5.97 \frac{\mu A}{cm^2}$



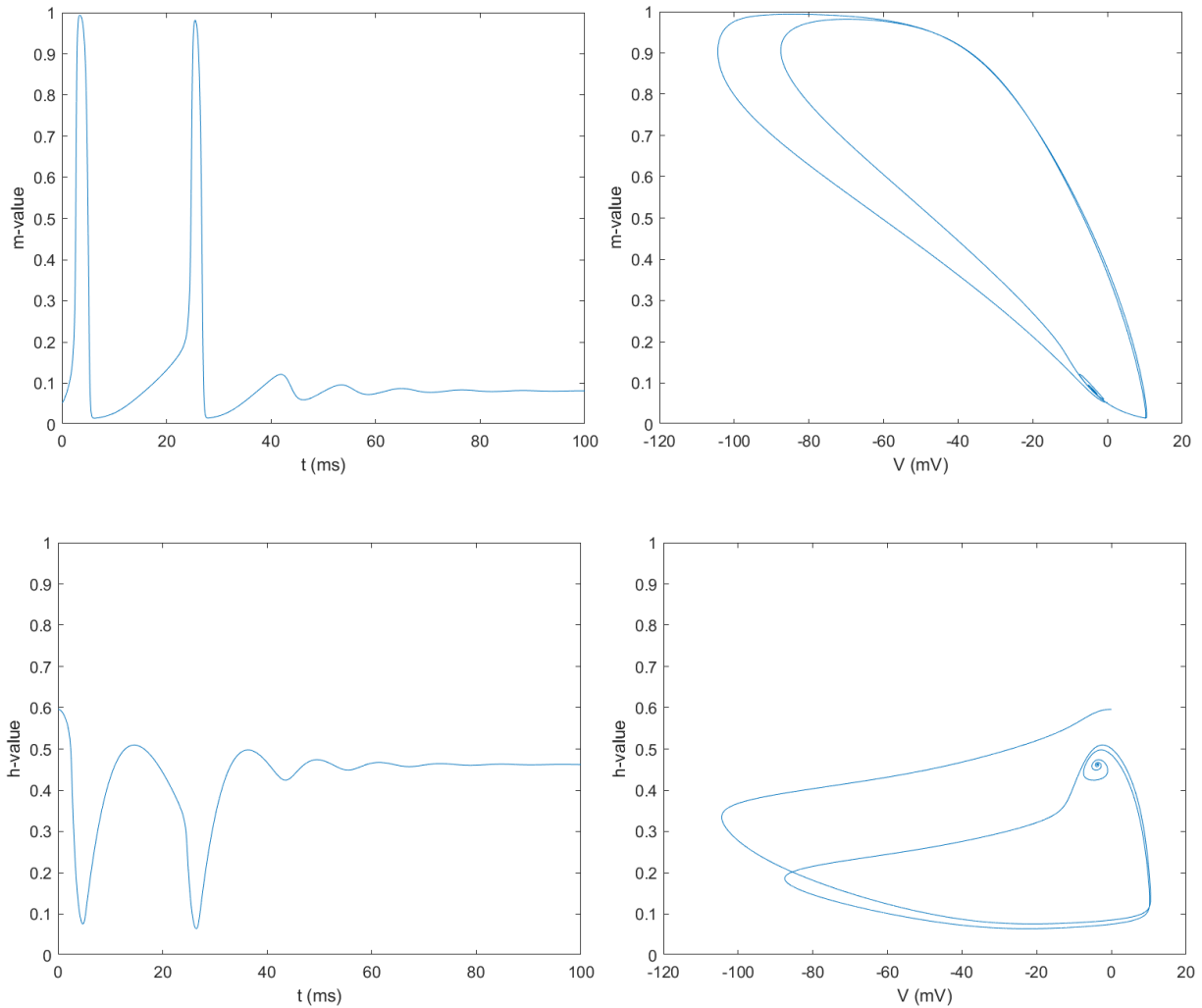


Figure 3.7. Gating variables vs. time and voltage at $i_{input} = 5.97 \frac{\mu A}{cm^2}$

The phase space plots in Figure 3.7 illustrate the ion channel dynamics for the two-peak threshold. The small spiral features in the n and h phase space plots at $V = 0$ represent the ripple voltage versus time behavior after 40ms.

4. Steady-state Action Potential Generation

With a sufficiently high current, action potentials are continuously regenerated after the refractory period (see Figures 3.8 and 3.9). The observed threshold is $i_{input} = 6.26 \frac{\mu A}{cm^2}$. The phase space plots (Figure 3.10) illustrate classic limit cycle behavior, consistent with the now oscillatory behavior of the membrane potential.

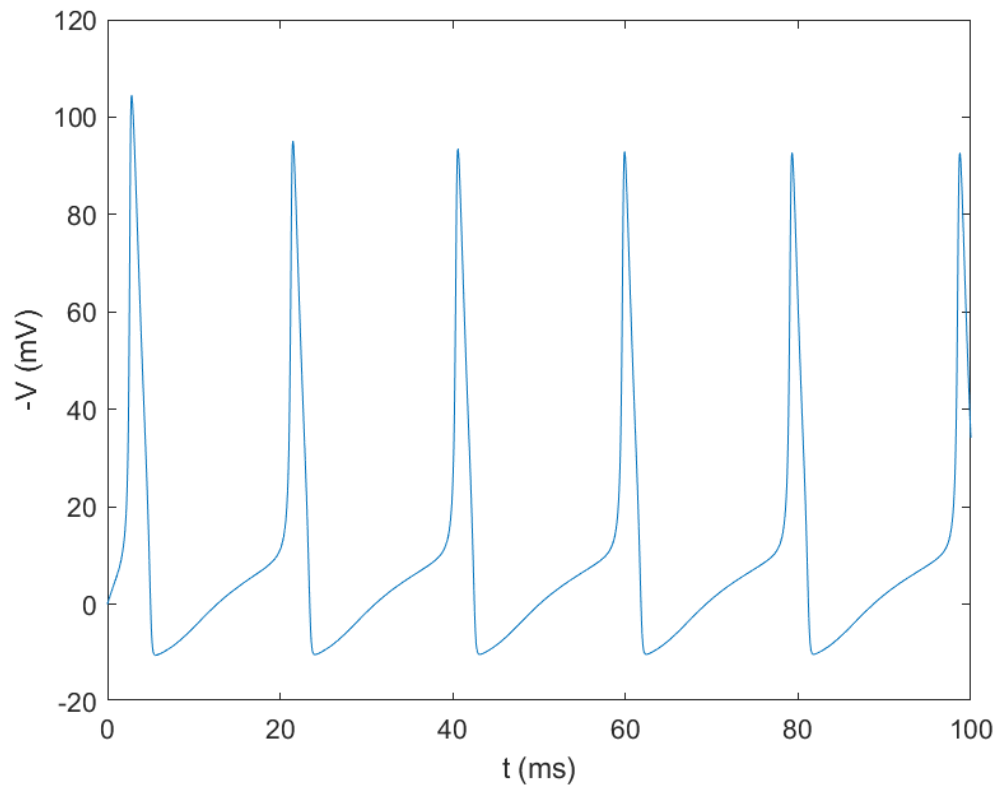


Figure 3.8. Steady-state action potential in the first 100ms for $i_{input} = 6.26 \frac{\mu A}{cm^2}$.

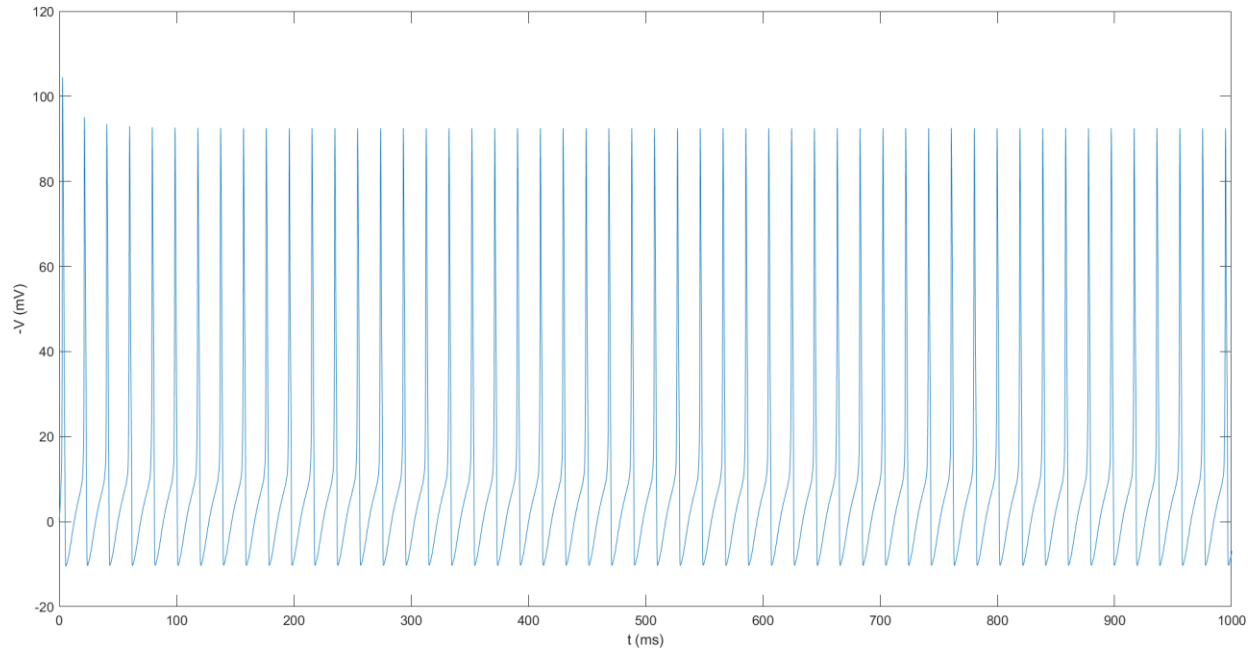
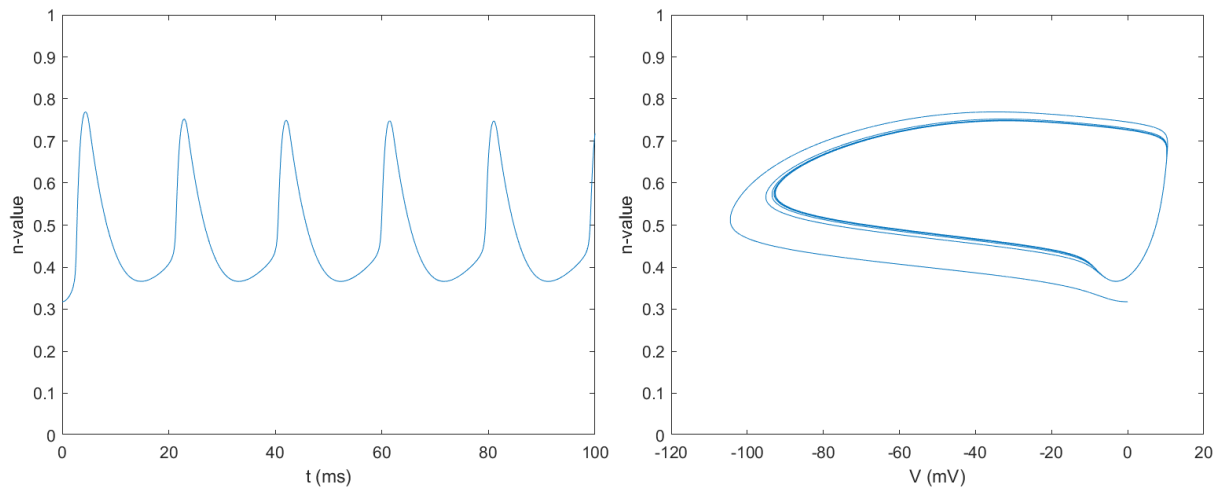


Figure 3.9. Steady-state action potential generation to 1000ms for $i_{input} = 6.26 \frac{\mu A}{cm^2}$.



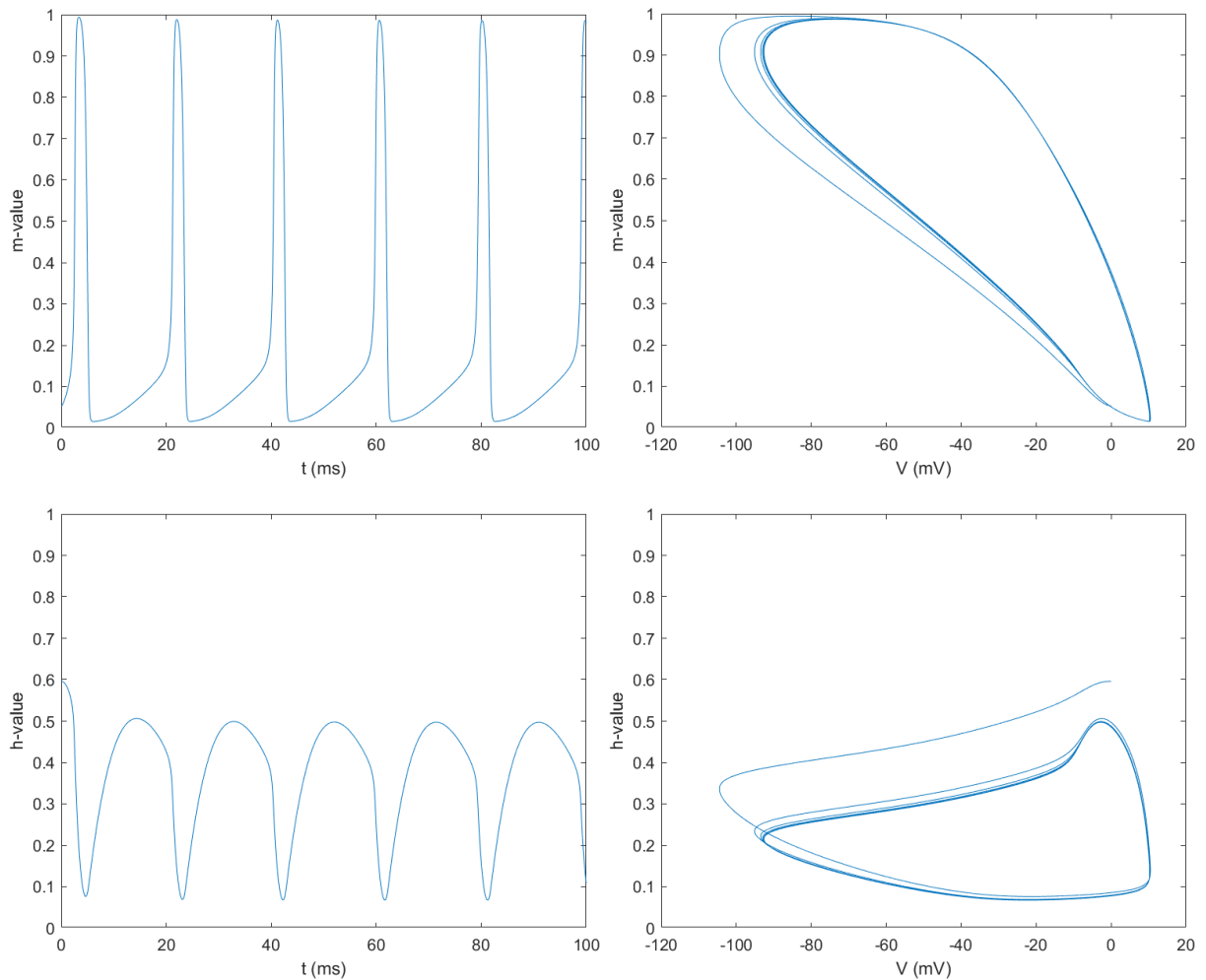


Figure 3.10. Gating variables vs. time and voltage at $i_{input} = 6.26 \frac{\mu A}{cm^2}$

Periodic phenomena can also be analyzed using Fourier analysis. In Figure 3.11 we show the fast Fourier transform of the periodic signal. The most salient feature is that the signal consists of a discrete set of frequencies, which is characteristic of non-chaotic phenomena. This is consistent with the limit cycles observed in Figure 3.10. Thus, despite the significant non-linearity of the HH equations, the solutions do not exhibit chaos, at least under the conditions of these solutions.

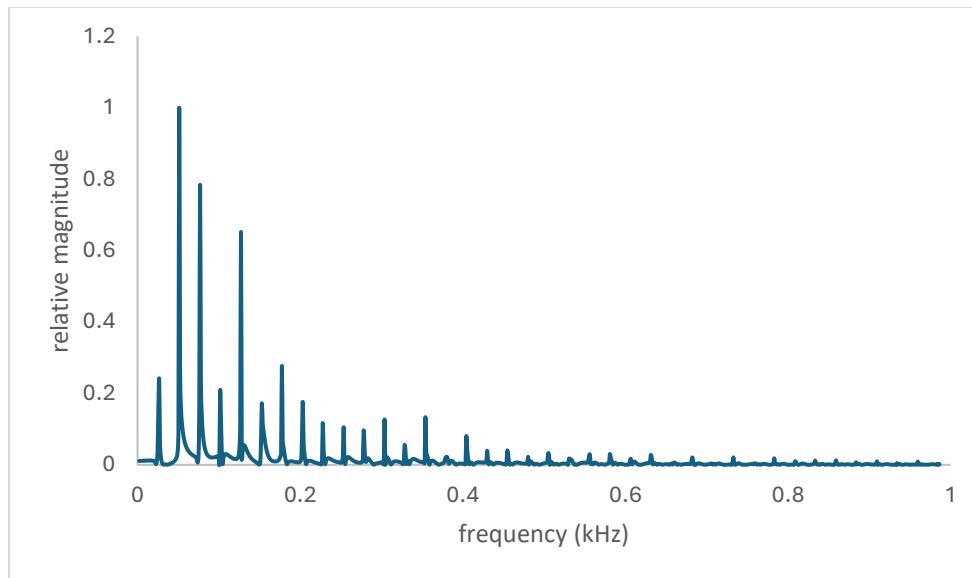


Figure 3.11. Fast Fourier transform of the periodic HH solution. The large dc peak at frequency = 0 has been suppressed for clarity.

To summarize, there are several key thresholds associated with the generation of action potentials. The results illustrate two important features of the Hodgkin Huxley model: the “all or nothing” characteristic of action potential generation, and the importance of the post-peak refractory period. Both of these characteristics are crucial for the role that action potentials play in neuron dynamics.

C. Sensitivity to Time Step

If the value of time step h in the Runge-Kutta method is too large, the results may not be accurate. However, with smaller h more time steps are needed for program execution and this can lead to computational times that are impractical. We tested the effect of h on our results in

several ways. A simple test is to vary h and compare the resulting voltage versus time plots. In addition, given the sensitivity of the model to the current threshold, we can also compare the threshold for single and multiple action potential generation. When h is sufficiently small, there will be no change in the results to within some acceptable difference by making h smaller. In our program we varied h from 0.01, 0.001, and 0.0001 mS. Table 3.1 give the results, where it is observed that there is very little difference in the results. Figure 3.12 shows the superimposed plots for the three cases, where to this resolution no difference between the plots.

Table 3.1. Current threshold, maximum potential, and time for maximum potential for the three cases $h = 0.01, 0.001, \text{ and } 0.0001$.

h (mS)	0.01	0.001	0.0001
Threshold current ($\mu\text{A}/\text{cm}^2$)	2.2382	2.2382	2.2382
maximum V (V)	11.28	11.281	11.2807
time at maximum V(mS)	91.12180	91.12191	91.12193

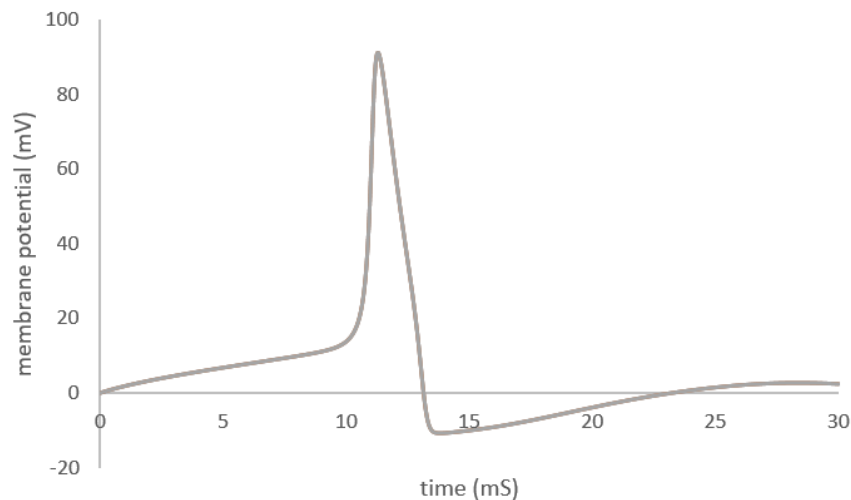


Figure 3.12. Superimposed action potential plots for different time steps

Chapter IV: Full Spatial-Temporal HH Equations

A. Introduction

1. Overview

In this chapter we will introduce the spatial dependence into the HH equations. The derivation of this equation, called the cable equation, is very similar to the equation that describes wave propagation along an electrical cable, except in this case the equation is first order in time rather than second order. As such it resembles a type of diffusion equation. Instead of the usual particle diffusion we can interpret the equation as a diffusion of voltage. This proposal will be discussed further below.

The following diagram illustrates the essential features of a propagating action potential.

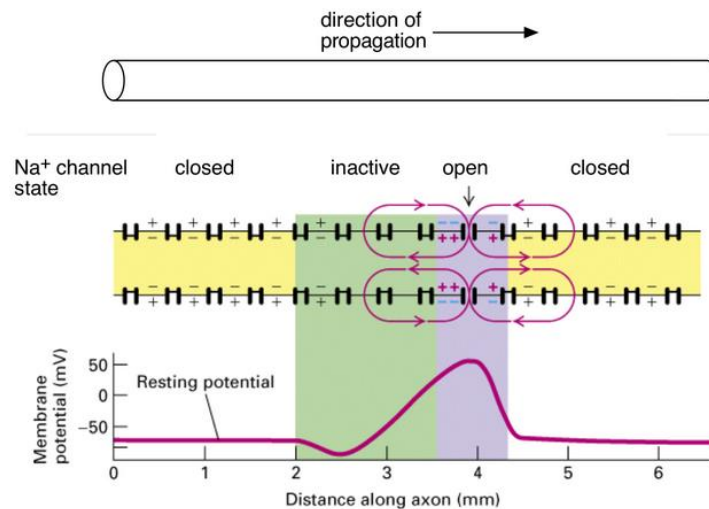


Figure 4.1. Essential features of a propagating action potential

Copyright © 2023 by Fred Rieke licensed under a [Creative Commons Attribution 4.0 International License](https://creativecommons.org/licenses/by/4.0/) <https://uw.pressbooks.pub/physiology/chapter/action-potential-propagation/>
 (Modified from Lodish, Molecular Cell Biology) [16]

In this illustration, the action potential is propagating to the right. As discussed in Chapter 2, the inactivation of the Na^+ channels following the action potential results in the unidirectional propagation of the pulse. The purpose of this chapter is to derive and (numerically) solve the HH model including spatial propagation. The approach is similar to that used in the derivation of the propagation of electromagnetic waves down a coaxial cable.

2. The Cable Equation

The derivation of the cable equation is based on the following equivalent circuit:

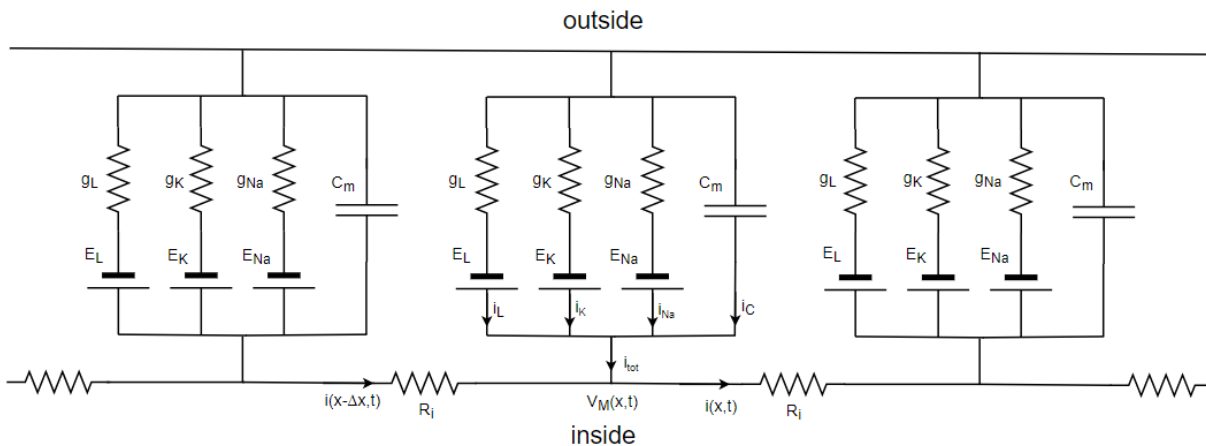


Figure 4.2. Equivalent Electrical Circuit Model (spatial consideration)

We can apply Kirchoff's node rule at x :

$$i(x - \Delta x, t) + i_{tot} = i(x, t)$$

so

$$i(x - \Delta x, t) - i(x, t) = -i_{tot}$$

where

$$i_{tot} = i_{Na} + i_K + i_L + i_C$$

giving

$$i(x - \Delta x, t) - i(x, t) = -i_{Na} - i_K - i_L - i_C$$

If we take the outside of the neuron to be at $V = 0$ we have

$$V_M(x, t) - E_{Na} + \frac{i_{Na}}{g_{Na}} = 0$$

$$V_M(x, t) - E_K + \frac{i_K}{g_K} = 0$$

$$V_M(x, t) - E_L + \frac{i_L}{g_L} = 0$$

which gives

$$-i_{Na} = g_{Na}(V_M(x, t) - E_{Na})$$

$$-i_K = g_K(V_M(x, t) - E_K)$$

$$-i_L = g_L(V_M(x, t) - E_L)$$

The voltage across the capacitor is related to the charge by

$$Q = C_M V(x, t)$$

so the capacitor current is

$$i_C = \frac{dQ}{dt} = C_M \frac{dV_M}{dt}$$

The node equation becomes

$$\begin{aligned}
i(x - \Delta x, t) - i(x, t) &= g_K(V_M(x, t) - E_K) + g_{Na}(V_M(x, t) - E_{Na}) + g_L(V_M(x, t) - V_L) \\
&\quad - C_M \frac{dV_M(x, t)}{dt}
\end{aligned}$$

We have

$$\frac{i(x - \Delta x, t) - i(x, t)}{\Delta x} \approx \frac{\partial i(x, t)}{\partial x}$$

$$\frac{\partial i(x, t)}{\partial x} = \frac{g_{Na}}{\Delta x} (V_M(x, t) - E_{Na}) + \frac{g_K}{\Delta x} (V_M(x, t) - E_K) + \frac{g_L}{\Delta x} (V_M(x, t) - E_L) - C_M \frac{dV_M(x, t)}{\Delta x dt}$$

Ohm's Law says:

$$V_M(x, t) - V_M(x + \Delta x, t) = i(x, t)R_i$$

But

$$\frac{V_M(x, t) - V_M(x + \Delta x, t)}{\Delta x} \approx -\frac{\partial V_M}{\partial x}$$

so

$$\frac{\partial V_M}{\partial x} = -\frac{i(x, t)R_i}{\Delta x}$$

Taking the derivative

$$\frac{\partial^2 V_M}{\partial x^2} = -\frac{R_i}{\Delta x} \frac{\partial i}{\partial x}$$

Substituting the current equation

$$\frac{\partial^2 V_M}{\partial x^2} = -\frac{R_i}{\Delta x} \left(\frac{g_{Na}}{\Delta x} (V_M(x, t) - E_{Na}) + \frac{g_K}{\Delta x} (V_M(x, t) - E_K) + \frac{g_L}{\Delta x} (V_M(x, t) - E_L) + \frac{C_M}{\Delta x} \frac{\partial V_M}{\partial t} \right)$$

Re-arranging gives

$$\frac{\partial V_M}{\partial t} = \frac{\Delta x^2}{C_M R_i} \frac{\partial^2 V_M}{\partial x^2} - \frac{g_K}{C_M} (V_M - E_K) - \frac{g_{Na}}{C_M} (V_M - E_{Na}) - \frac{g_L}{C_M} (V_M - E_L)$$

The term

$$\frac{\Delta x^2}{C_M R_i}$$

can be reformulated as

$$\frac{1}{c_m r_i}$$

Where c_m is the capacitance per unit length and r_i is the longitudinal resistance per unit length.

This term has units of cm^2/s and represents an effective diffusion constant for the voltage.

Defining

$$D = \frac{1}{c_m r_i}$$

and substituting the expressions for g_K and g_{Na} from Chapter 2 we have

$$\frac{\partial V_M}{\partial t} = D \frac{\partial^2 V_M}{\partial x^2} - \frac{\bar{g}_K}{C_M} n^4 (V_M - E_K) - \frac{\bar{g}_{Na}}{C_M} m^3 h (V_M - E_{Na}) - \frac{g_L}{C_M} (V_M - E_L) \quad (4.1)$$

Or

$$\frac{\partial V_M}{\partial t} = D \frac{\partial^2 V_M}{\partial x^2} - f(V_M) \quad (4.2)$$

which has the form of a diffusion equation for voltage having a nonlinear “source term” $f(V_M)$.

We would therefore expect that the solutions for V_M would correspond to a kind of “voltage diffusion” down the axon, with the nonlinear term $f(V_M)$ that in some sense counters the dissipation (or perhaps, more accurately, the entropy generation) that accompanies usual particle diffusion. Below we present some evidence for this interpretation.

B. Numerical Implementation

Equation 4.1 (coupled to the associated rate equations for n , m , and h described in Chapter 2) is a boundary value problem in space and time. There are various methods of solving such equations numerically. In this work we apply the explicit method. The explicit method uses the results of the previous time step to calculate the quantities in the current time step. The voltage for $t = 0$ is given everywhere including the boundaries as an initial condition. For the next time step $t = \Delta t$, the voltage is calculated at each interior point using the values at the previous time step of $t = 0$, while keeping the boundary conditions fixed. At $t = 2\Delta t$, the voltage is calculated at each interior point using the values at the previous time step $t = \Delta t$, again keeping the boundary conditions fixed. And so on. In this way the equation is solved with both the initial and boundary conditions satisfied. The method can be illustrated by the following diagram:

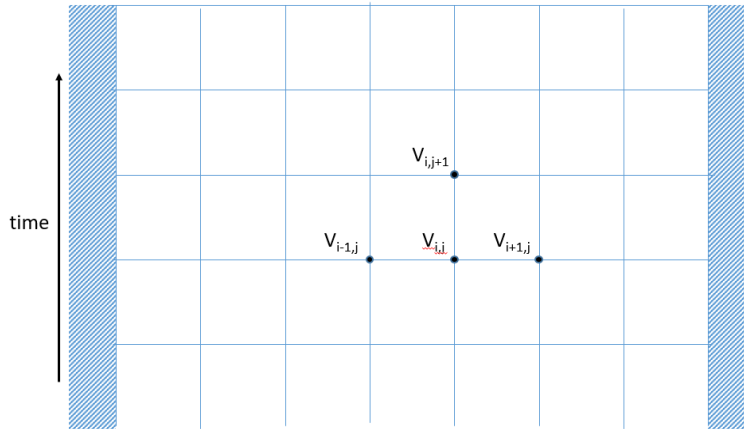


Figure 4.3. Diagram of the explicit method

The explicit method is commonly used because of its simplicity, but accurate solutions require a large number of small time steps. In a sense the explicit method is analogous to the Euler method for solving initial value differential equations. There are more accurate methods that result in a smaller error for a given time step, such as the well-known Crank-Nicholson method. In our case we chose to focus on the explicit method since it is more easily adaptable for introducing stochastic effects (see Chapter 5). Below we will further consider the effect of the space and time step sizes.

1. Derivation of the Finite Difference Equations

To numerically solve Equation 4.2 (together with the accompanying channel equations 2.8 through 2.14) we need to convert the equations into finite difference equations. We have from above:

$$\frac{\partial V_M}{\partial t} = D \frac{\partial^2 V_M}{\partial x^2} - f(V_M)$$

where

$$f(V_M) = \frac{\bar{g}_K}{C_M} n^4 (V_M - E_K) - \frac{\bar{g}_{Na}}{C_M} m^3 h (V_M - E_{Na}) - \frac{g_L}{C_M} (V_M - E_L)$$

Note that n , m , and h also depend on V_M . For the time derivative at the i th position and j th time step we can do the usual Taylor expansion

$$V_{i,j+1} = V_{i,j} + \delta T \left(\frac{\partial V}{\partial T} \right)_{i,j} + O(\delta T^2)$$

So

$$\left(\frac{\partial V}{\partial T} \right)_{i,j} = \frac{V_{i,j+1} - V_{i,j}}{\delta T}$$

For the second order spatial derivative we have

$$V_{i+1,j} = V_{i,j} + \delta X \left(\frac{\partial V}{\partial X} \right)_{i,j} + \frac{1}{2!} \delta X^2 \left(\frac{\partial^2 V}{\partial X^2} \right)_{i,j} + O(\delta X^3)$$

$$V_{i-1,j} = V_{i,j} - \delta X \left(\frac{\partial V}{\partial X} \right)_{i,j} + \frac{1}{2!} \delta X^2 \left(\frac{\partial^2 V}{\partial X^2} \right)_{i,j} + O(\delta X^3)$$

Adding these equations

$$V_{i+1,j} + V_{i-1,j} = 2V_{i,j} + 2 \frac{1}{2} \delta X^2 \left(\frac{\partial^2 V}{\partial X^2} \right)_{i,j}$$

So

$$\left(\frac{\partial^2 V}{\partial X^2} \right)_{i,j} = \frac{V_{i+1,j} - 2V_{i,j} + V_{i-1,j}}{\delta X^2}$$

Then

$$\frac{\partial V_M}{\partial T} = D \frac{\partial^2 V_M}{\partial X^2} - \frac{\bar{g}_K}{C_M} n^4 (V_M - E_K) - \frac{\bar{g}_{Na}}{C_M} m^3 h (V_M - E_{Na}) - \frac{g_L}{C_M} (V_M - E_L)$$

Becomes

$$\frac{V_{i,j+1} - V_{i,j}}{\delta T} = \frac{V_{i+1,j} - 2V_{i,j} + V_{i-1,j}}{\delta X^2} - f(V_{i,j})$$

So

$$V_{i,j+1} = V_{i,j} + \frac{\delta T}{\delta X^2} (V_{i+1,j} - 2V_{i,j} + V_{i-1,j}) - \delta T f(V_{i,j})$$

Including the explicit form for $f(V_M)$

$$V_{i,j+1} = V_{i,j} + r(V_{i+1,j} - 2V_{i,j} + V_{i-1,j}) - \delta T \left(\frac{\bar{g}_K}{C_M} n^4 (V_{i,j} - E_K) - \frac{\bar{g}_{Na}}{C_M} m^3 h (V_{i,j} - E_{Na}) - \frac{g_L}{C_M} (V_{i,j} - E_L) \right)$$

where

$$r = \frac{\delta T}{\delta X^2}$$

As with the space-clamped problem discussed in Chapter 2 and 3, in experimental situations it is often convenient to add an external current as a convenient way to initiate the excitation. In that case the complete cable difference equation would be

$$V_{i,j+1} = V_{i,j} + r(V_{i+1,j} - 2V_{i,j} + V_{i-1,j}) - \delta T \left(\frac{\bar{g}_K}{C_M} n^4 (V_{i,j} - E_K) - \frac{\bar{g}_{Na}}{C_M} m^3 h (V_{i,j} - E_{Na}) - \frac{g_L}{C_M} (V_{i,j} - E_L) \right) + \delta T \frac{I}{C_m} \quad (4.3)$$

For the channel equations we have as before

$$\frac{dn}{dT} = \alpha_n(V)(1 - n) - \beta_n(V)n$$

Now

$$\left(\frac{dn}{dT}\right)_{i,j} = \frac{n_{i,j+1} - n_{i,j}}{\delta T}$$

So

$$\begin{aligned} \frac{n_{i,j+1} - n_{i,j}}{\delta T} &= \alpha_n(V_{i,j})(1 - n_{i,j}) - \beta_n(V_{i,j})n_{i,j} \\ n_{i,j+1} &= n_{i,j} + \delta T[(\alpha_n(V_{i,j})(1 - n_{i,j}) - \beta_n(V_{i,j})n_{i,j})] \end{aligned} \quad (4.4)$$

with similar equations for m and h. The equations for α_i and β_i are the same as previously described in Chapter 2.

$$\alpha_n(V) = \frac{0.01(V + 10)}{\exp\left(\frac{V + 10}{10}\right) - 1} \text{ msec}^{-1}$$

$$\beta_n(V) = 0.125 \exp\left(\frac{V}{80}\right) \text{ msec}^{-1}$$

$$\alpha_m(V) = \frac{0.1(V + 25)}{\exp\left(\frac{V + 25}{10}\right) - 1} \text{ msec}^{-1}$$

$$\beta_m(V) = 4 \exp\left(\frac{V}{18}\right) \text{ msec}^{-1}$$

$$\alpha_h(V) = 0.07 \exp\left(\frac{V}{20}\right) \text{ msec}^{-1}$$

$$\beta_h(V) = \frac{1}{\exp\left(\frac{V + 30}{10}\right) + 1} \text{ msec}^{-1}$$

2. Boundary Conditions, Spatial and Temporal Resolution

There are several possibilities for boundary conditions. With Dirichlet boundary conditions, the value of V_M is specified on the boundaries. For Neumann boundary conditions, the slope of V_M at the boundaries is specified. For mixed boundary conditions, a relation between the value and the slope is specified at the boundary. The choice of boundary conditions is in general prescribed by the conditions of the experiment. Both Dirichlet and Neumann boundary conditions have been employed in HH studies and we have considered both in our work. However, for the purposes of this study it makes no difference which conditions are used. We have therefore chosen to focus on Dirichlet conditions as a somewhat more intuitive approach. The boundary conditions used for the results below are $V(0,t) = 0$ and $V(L, t) = 0$, except for the first 1 ms where $V(0, t < 1\text{ms}) = V_0$ and V_0 is a voltage above the threshold voltage for initiating an action potential.

As with all finite difference reductions of differential equations, attention must be given to the effects of the intervals used in the calculation. In the present case there are two relevant intervals: the spatial interval δX and the temporal interval δT . In studies of the diffusion equation, it has been shown that for a stable and convergent solution we must have (Morton thesis page 17 [15]),

$$\frac{\delta T}{D \delta X^2} < 0.5$$

If we chose a value of δX , we can find δT according to

$$\delta T < \frac{D \delta X^2}{2}$$

In our case we opted for a more conservative criteria (recognizing that the *accuracy* of the explicit method requires a small time step) and chose δT as

$$\delta T = \frac{D \delta X^2}{6}$$

The effect of the choice of δX will be discussed below.

C. Results

Figure 4.4 shows a typical solution of Equation 4.3 with $D = 0.04 \text{ cm}^2/\text{mS}$ and $\delta X = 0.01 \text{ cm}$.

The action potential propagates down the axon after the initial excitation at $x = 0$ and $t < 1 \text{ ms}$.

The presence of the refractory part is apparent on the trailing edge of the voltage spike. In Figure

4.5 the peak position versus time is given for the three cases of $\delta X = 0.05 \text{ cm}$, 0.025 cm , and

0.01 cm . The spike is observed to propagate at a constant speed after initiation. There is a small

but measurable difference between the $\delta X = 0.025 \text{ cm}$ case and the $\delta X = 0.01 \text{ cm}$ case. For $\delta X =$

0.01 cm the runtime of the MATLAB program is about 1 hour for the 200 ms case. Values of δX

smaller than 0.01 cm start to become impractical due to the program runtime (note that the time

interval decreases very quickly as δX is decreased). Of course this is not an intrinsic limitation,

but a better way to decrease the runtime would be to use a more efficient algorithm (for example

the Crank-Nicholson method) and/or use a compiled language (such as C++) instead of the

interpreted language MATLAB. Nevertheless, our results do not seem to have a significant

dependence on δX for $\delta X \leq 0.025 \text{ cm}$ (Figure 4.5).

The results in Figure 4.5 confirm that the action potential propagates at a constant speed, in this case a speed of $0.4243 \text{ cm/ms} = 424.3 \text{ cm/s}$ ($\delta X = 0.01 \text{ cm}$). This is close to the experimental speed observed by Hodgkin and Huxley (HH 1952) of 1070 cm/s . This speed occurs after a short latency period of $\Delta t = \frac{0.6207}{0.4243} = 1.463 \text{ ms}$ apparently required to establish the action potential, as implied by the non-zero intercepts in Figure 4.3. This is apparently the time it takes to establish a propagating action potential for the 1.0 ms initial voltage.

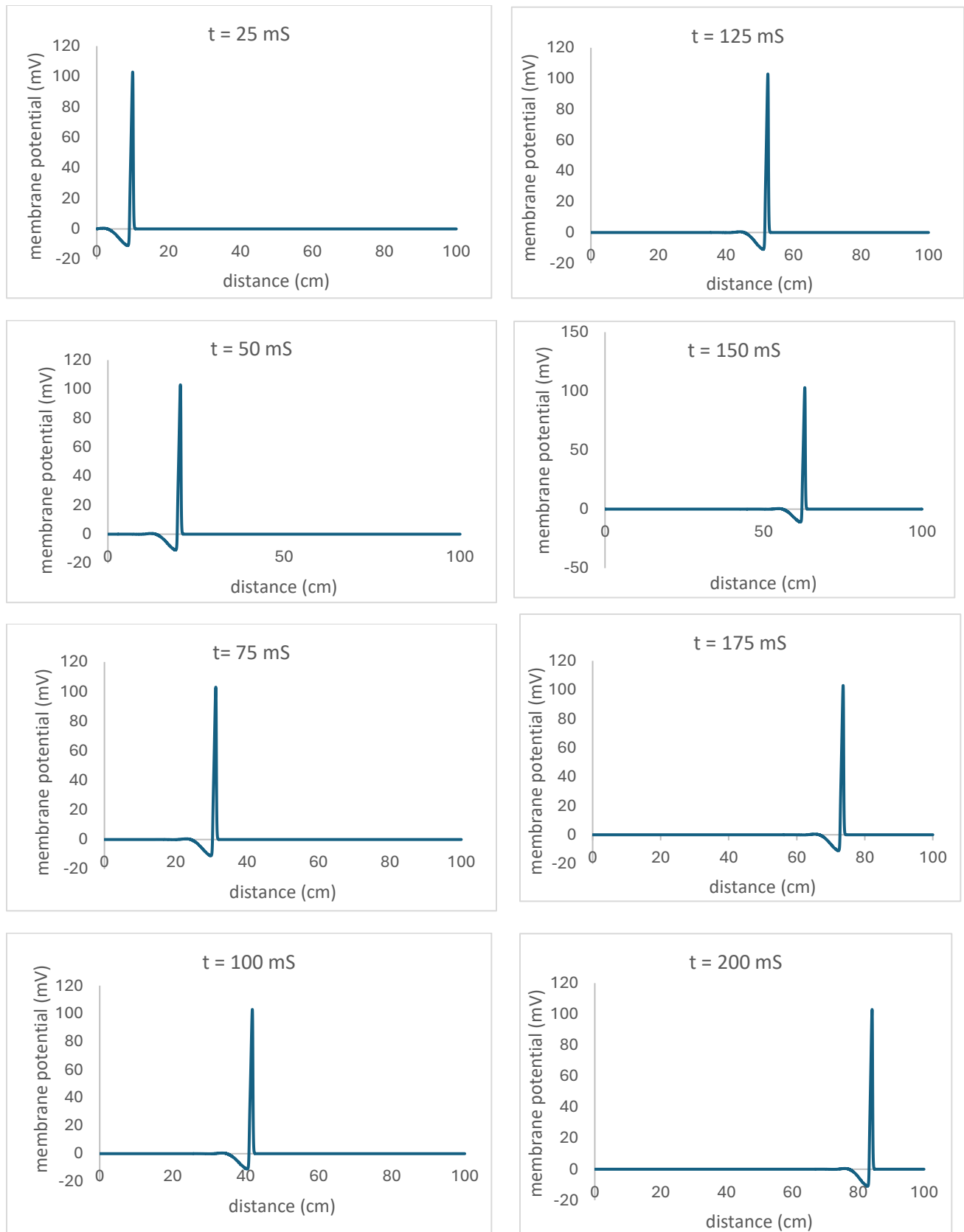


Figure 4.4. Action potential propagation for $D = 0.04 \text{ cm}^2/\text{s}$.

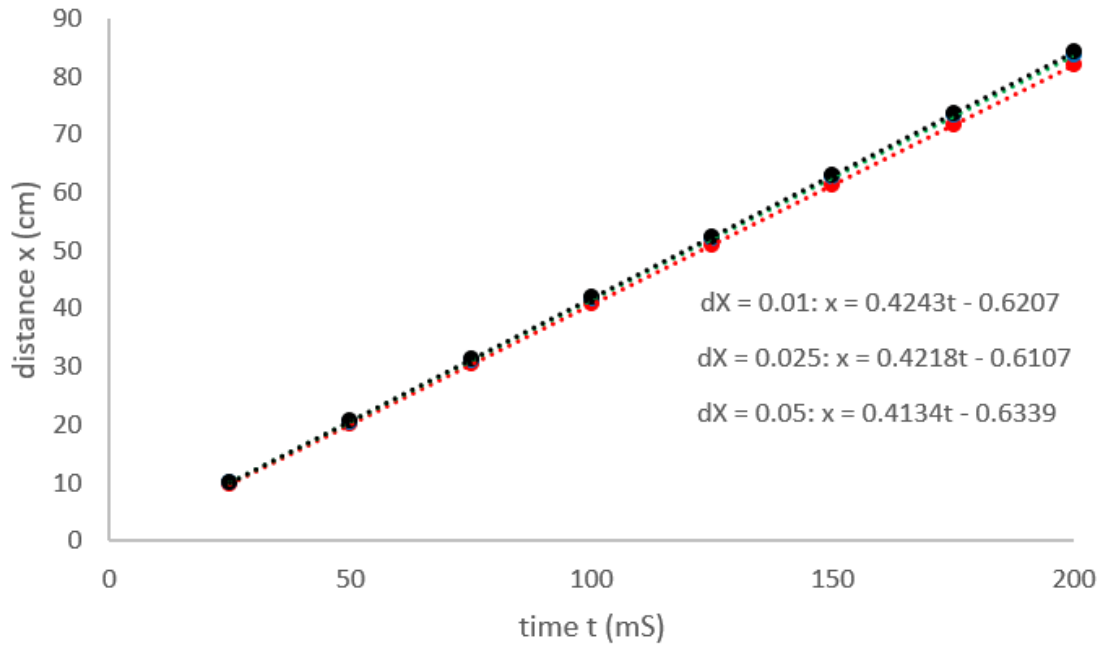


Figure 4.5. Distance versus time for different values of δx . $D = 0.04 \text{ cm}^2/\text{s}$

1. Diffusion Aspects of the HH Model

As mentioned above, the HH voltage equation has the mathematical form of a (non-linear) diffusion equation. It is therefore of interest to explore in what ways the solutions demonstrate diffusion effects. Surprisingly, this aspect of the HH model does not seem to have received much attention in the literature, at least quantitatively. One often finds the statement the HH represents a voltage diffusion phenomena, but we have not been able to find any kind of mathematical justification of this idea. Below we present an interpretation of what may be meant by voltage diffusion in the HH model, and how this diffusion contrasts with classical (Fickian) particle diffusion.

In ordinary particle diffusion without sinks or sources, the diffusion equation is

$$\frac{\partial n}{\partial t} = D \frac{\partial^2 n}{\partial x^2}$$

For a point source at the origin, it is easy to verify the solution for $t > 0$ is a Gaussian centered at the origin that spreads in time:

$$n(x, t) = \frac{M}{2\sqrt{\pi Dt}} e^{-\frac{x^2}{4Dt}}$$

where M is the total mass of the diffusing particles. The characteristic distance over which the particles have diffused in time t is given by:

$$\Delta x = \sqrt{4Dt} \quad (4.5)$$

which can be interpreted as the mean distance the particles have diffused in time t . This is the well-known “square root” relation between space and time in diffusion (or generally random walk or Brownian motion) phenomena. Solutions for $n(x, t)$ at different times is shown in Figure 4.6.

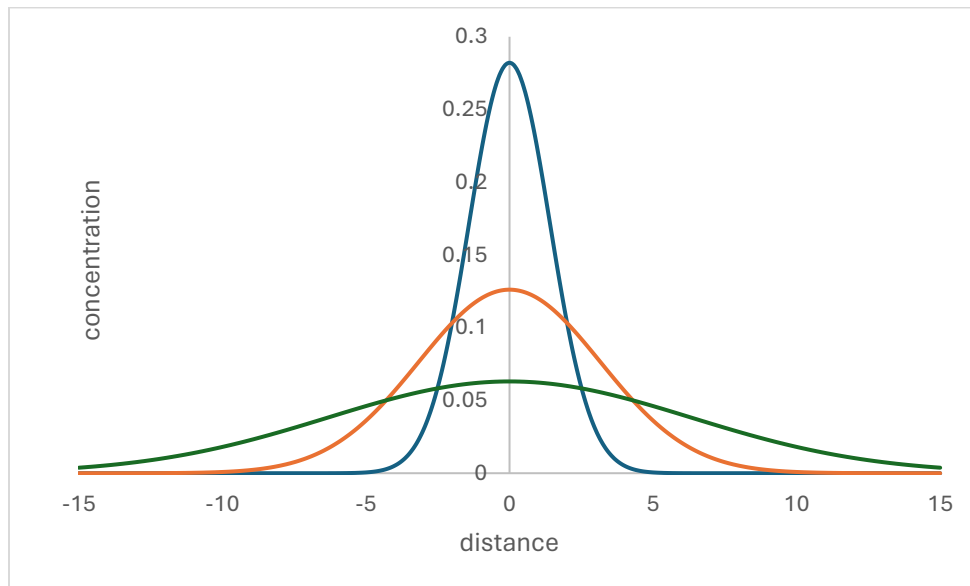


Figure 4.6. Linear diffusion (Equation 4.6) with $v = 0$ at times $t = 1, 5,$ and 20 units ($D = 1$)

Returning to the HH equation, it is interesting to examine in what way the relationship Equation 4.5 can apply. Figure 4.7 shows the action potential for at $t = 100$ ms for $D = 0.005, 0.01, 0.02, 0.04,$ and 0.08 cm^2/s . In Figure 4.7 we have plotted the action potential as a function of the diffusion coefficient at a fixed time of 100 ms. In Figure 4.8 we have plotted the distance travel in 100 ms versus D . From the fit we see that the distance traveled in this fixed time goes exactly as \sqrt{D} as predicted by Equation 4.5. The proportionality factor is much large than that predicted by Equation 4.5, with 209.56 cm from the data fit compared to $\sqrt{4 \times 100} = 20$ cm predicted from Equation 4.5. Nonetheless, the close agreement with the functional dependence on D is striking.

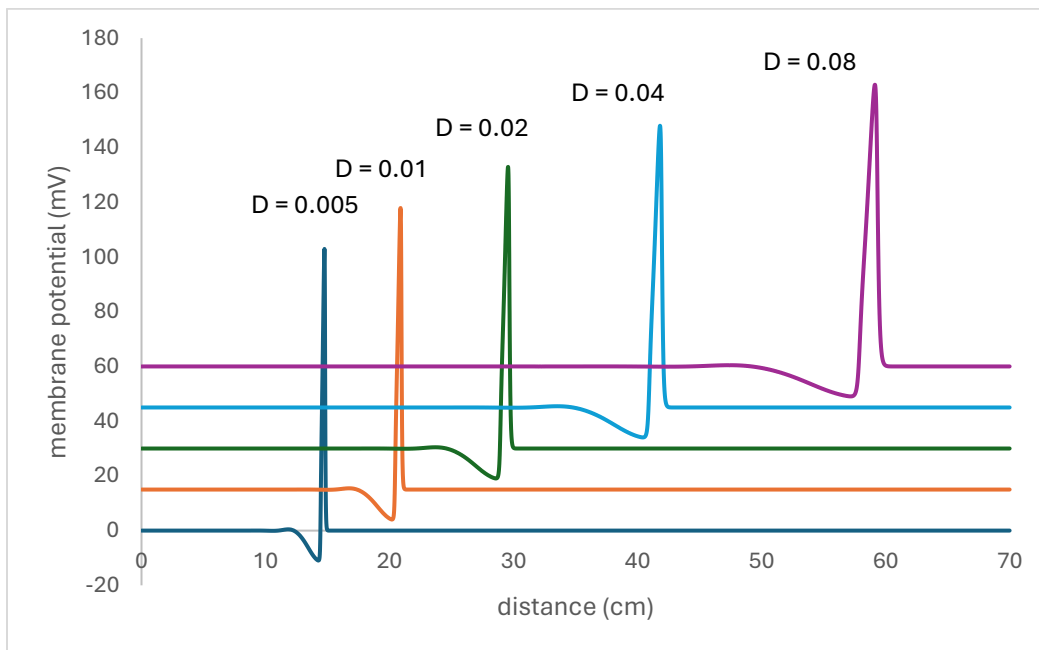


Figure 4.7. Action potentials for various values of D (in cm^2/s) at 100 ms. The curves have been offset from $V_M = 0$ for clarity.

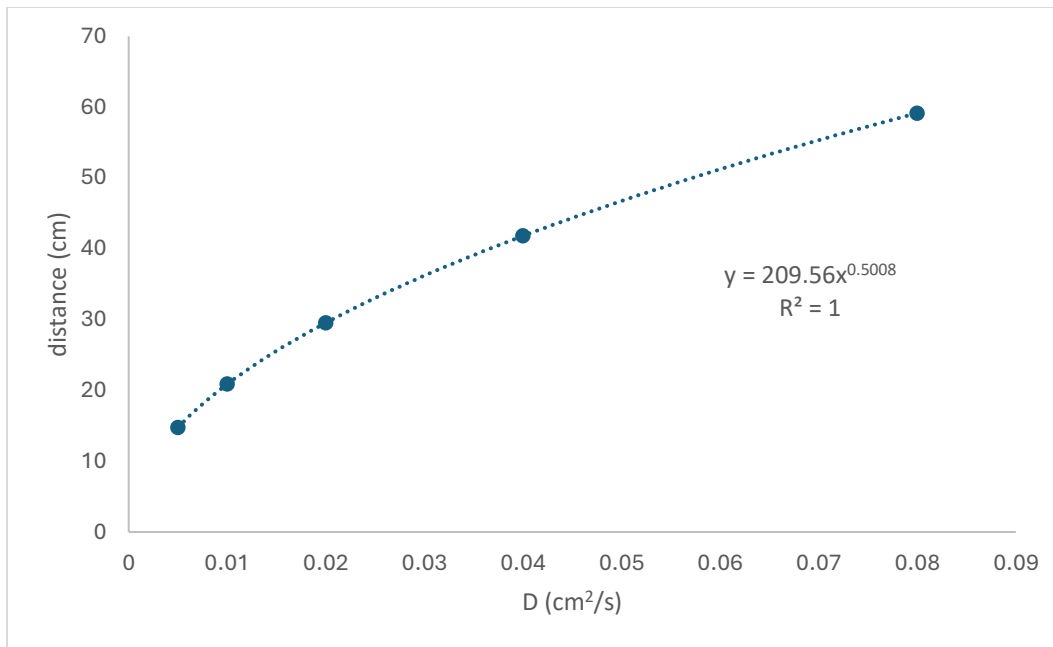


Figure 4.8. Peak position versus D for the data in Figure 4.6.

Another observation from the data in Figure 4.7 is the widening of the width of the action potential with increasing D . If we define the width of the pulse to be the full width at half maximum, we can examine its relationship with D . These results are plotted in Figure 4.9. Again, it is striking that the width of the pulse scales almost exactly with \sqrt{D} . However, it is important to point out that this does not represent a “spreading” of the pulse *in time* (as one expects in an actual Fickian diffusion process – see Figure 4.6). In fact, from Figure 4.6 we see that there is no spreading of the action potential with time.

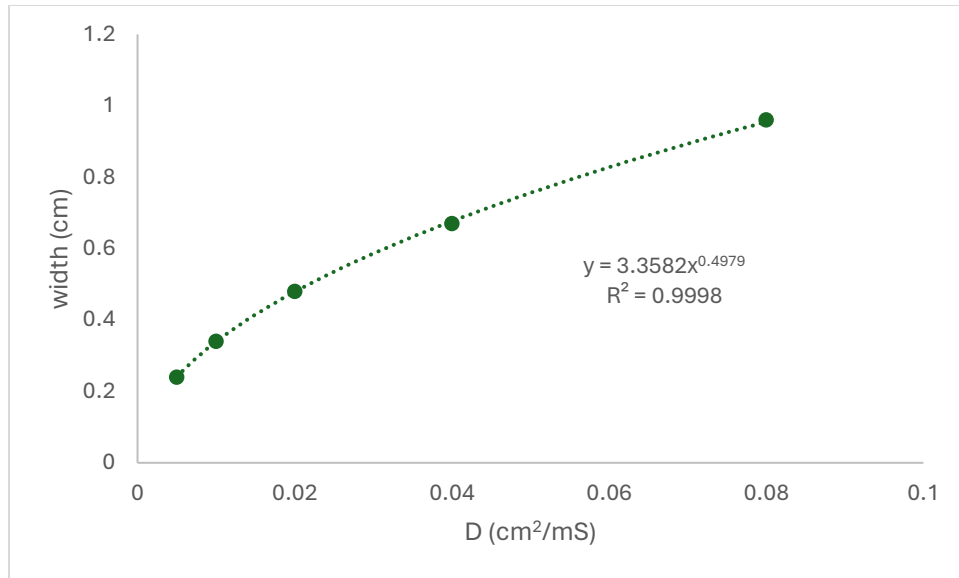


Figure 4.9. Pulse peak full width at half maximum versus D for the data in Figure 4.6.

We see that the diffusional nature of the action potential is manifested in the propagation speed's as well as the width of the action potential's dependence on D , the effective diffusion constant. However, we must be careful not to over-interpret these results. The diffusion of the voltage in the action potential *is not* a classical Fickian diffusion problem. The closest analog might be obtained by adding a drift term to the diffusion term. In that case we have:

$$\frac{\partial n}{\partial t} = D \frac{\partial^2 n}{\partial x^2} - v \frac{\partial n}{\partial t} \quad (4.6)$$

giving a solution

$$n(x, t) = \frac{M}{2\sqrt{\pi Dt}} e^{-\frac{(x-vt)^2}{4Dt}}$$

which can be verified by making the substitution

$$x \rightarrow x - vt$$

This solution represents a Gaussian propagating in the $+x$ direction with constant speed v . For the pulse moving in space, the characteristic behavior of this solution is that for a fixed value of the diffusion constant the Gaussian does not retain its shape and over time and space spreads out in space (see Figure 4.10).

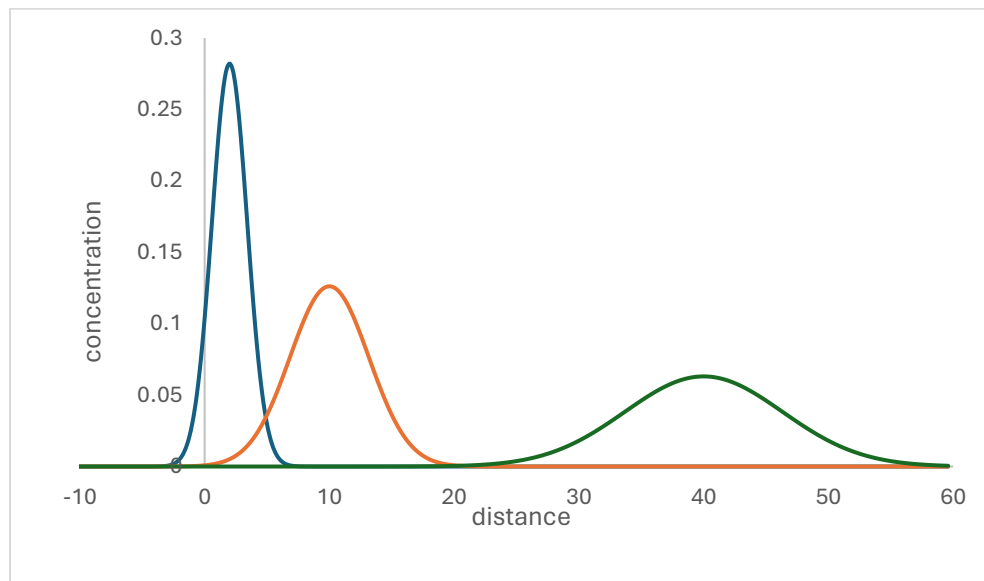


Figure 4.11. Linear diffusion (Equation 4.6) with $v = 2$ at times $t = 1, 5,$ and 20 units ($D = 1$)

However, there are significant differences between this solution and the HH solutions. First, in classical Fickian diffusion there is no dependence of the propagation speed v on D ; rather v is an independently specified parameter. Secondly, in this solution the Gaussian pulse spreads with time, as noted above, does not occur with the HH solution. Of course, the main difference between Equation 4.6 and the HH equation is that the Fickian diffusion with drift Equation 4.6 is linear, whereas the HH equation is non-linear due to the dependences of the channel variables n , m and h on V . Apparently, these non-linear terms serve to “counter” the spreading of the pulse that would be expected with classical random walk diffusion while still maintaining a constant propagation speed.

As far as we are aware there is no general theory of non-linear diffusion phenomena, at least none that we have encountered in the HH/action potential literature. If this is such a theory, it is beyond the scope of this paper, and the results presented here perhaps might serve as some experimental support for a more rigorous theoretical treatment.

In summary, there is an important sense that the action potential represents a type of voltage diffusion. The propagation speed and the width of the voltage pulse both exhibit a Fickian \sqrt{D} dependence. However, the pulse does not exhibit the random walk spreading in time characteristic of particle diffusion. Rather, the pulse propagates with constant width, implying that the non-linear channel terms counter the spreading of the pulse expected from the linear terms in the voltage equation. It is perhaps surprising that these features of the HH equation do not seem to have been noticed (or at least recorded) in the literature. The reason might simply be that for a *given neuron*, there is no reason to think that D would take on different values. Recall that D is given by

$$D = \frac{1}{c_m r_i}$$

where c_m and r_i are the membrane capacitance per unit length and the longitudinal resistance per unit length respectively. For a given cell, there is no obvious mechanism where these parameters would vary. In any case, the results here are an attempt to clarify in a more precise sense what it means for the HH model to exhibit voltage diffusion.

Chapter V: Extension of the HH Model and Future Work

A. Introduction

Our original goal in this work was to study stochastic effects in action potential models, by converting the HH equations into a set of stochastic equations. Stochastic effects are common in biophysical systems. For example, in action potentials stochastic effects are present in the dynamics of the voltage-gated ion channels. The opening and closing of these channels is ultimately a statistical problem, with the equations for n , m , and h in the HH model actually representing average behavior over large number of channels. Indeed, this is a frequent criticism of the applicability of the HH equation, that these stochastic effects are not explicitly included in the basic theory.

The theory of stochastic differential equations is highly developed. However, the theory is complex and application of these methods to non-linear problems such as the HH equations can be very challenging. The main issue is that stochastic terms do not have well-defined derivatives, so advanced methods of analysis (for example the Ito calculus) are required to solve the equations. One of the simplest approaches is the Euler–Maruyama method, which adds stochastic terms to the Euler algorithm as follows:

$$Y_{t+\Delta t} = Y_t + a(Y_t, t)\Delta t + b(Y_t, t)\Delta W_t$$

where ΔW_t is Wiener process that represents a kind of Brownian motion and $b(Y_t, t)$ depends on the nature of the stochasticity. In the most basic formulation ΔW_t can be represented as

$$\Delta W_t = z_i \sqrt{\Delta t}$$

where z_i is a pseudo-random number between 0 and 1. The square root dependence is reminiscent (and ultimately related to) the basic relation 4.5, which itself is a consequence of the random walk nature of Brownian diffusion

$$\Delta x = \sqrt{4Dt} \quad (4.5)$$

We can incorporate terms like $b(V_t, t)\Delta W_t$ in the HH model, but it is not a trivial matter to determine the correct form for $b(V_t, t)$. For example, in applying this approach to the channel equations, the $b(V_t, t)$ will depend in a complex way on the rate constants α_i and β_i . In this preliminary work, we will greatly simplify the dynamics and treat b as a constant that specifies the strength of the stochastic effects. We will consider a modified form of the voltage equation as follows:

$$V_{i+1} = V_i - \left[\frac{g_K}{C_M}(V_i - E_K) - \frac{g_{Na}}{C_M}(V_i - E_{Na}) - g_L \frac{g_K}{C_M}(V_i - E_L) + \frac{I}{C_M} \right] + \sigma z_i \sqrt{dT}$$

where the last term represents a stochastic contribution to the membrane voltage. In this simple example the channel equations are unchanged. A physical interpretation of this equation is that the last term represents voltage fluctuations caused by fluctuations in ions that do not participate in the action potential.

We can now consider the effects the stochastic term has on the threshold potential for a single action potential. Figures 5.1 and 5.2 give the results. First, we note that without the stochastic term, the threshold for initiating an action potential is very sharp (Figure 5.1). When stochasticity is added, the value of σ has a strong effect on the value of the threshold current for a successful action potential (recall that the threshold with no stochastic term is $2.24 \frac{\mu A}{cm^2}$). In

addition, near the threshold there is now a distribution of probability for successful action potentials versus current. For the case of $\sigma = 0.005 \text{ mV/ms}^{1/2}$, a current of $3.035 \frac{\mu\text{A}}{\text{cm}^2}$ is needed to reliably initiate an action potential (Figure 5.2). Below this value, there is a non-zero probability that an action potential will be initiated, down to a lower threshold of $3.031 \frac{\mu\text{A}}{\text{cm}^2}$ when no action potentials will be generated. For $\sigma = 0.05 \text{ mV/ms}^{1/2}$, reliable success for action potentials requires a current of $10.158 \frac{\mu\text{A}}{\text{cm}^2}$, but there is a decreasing non-zero probability that an action potential can occur down to $10.140 \frac{\mu\text{A}}{\text{cm}^2}$ (Figure 5.3). In addition to the shift in threshold for initiating action potentials, the range over which an action potential can be generate with probability less than one also increases with increasing σ ($0.004 \text{ mV/ms}^{1/2}$ in the case of $\sigma = 0.005 \text{ mV/ms}^{1/2}$, and $0.018 \text{ mV/ms}^{1/2}$ in the case of $\sigma = 0.05 \text{ mV/ms}^{1/2}$).

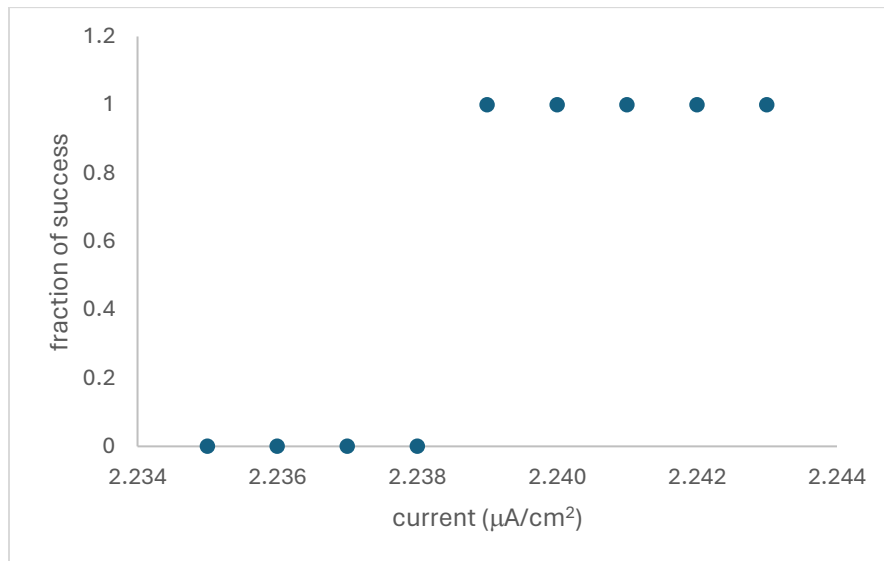


Figure 5.1. Success rate for action potential firing with no stochasticity

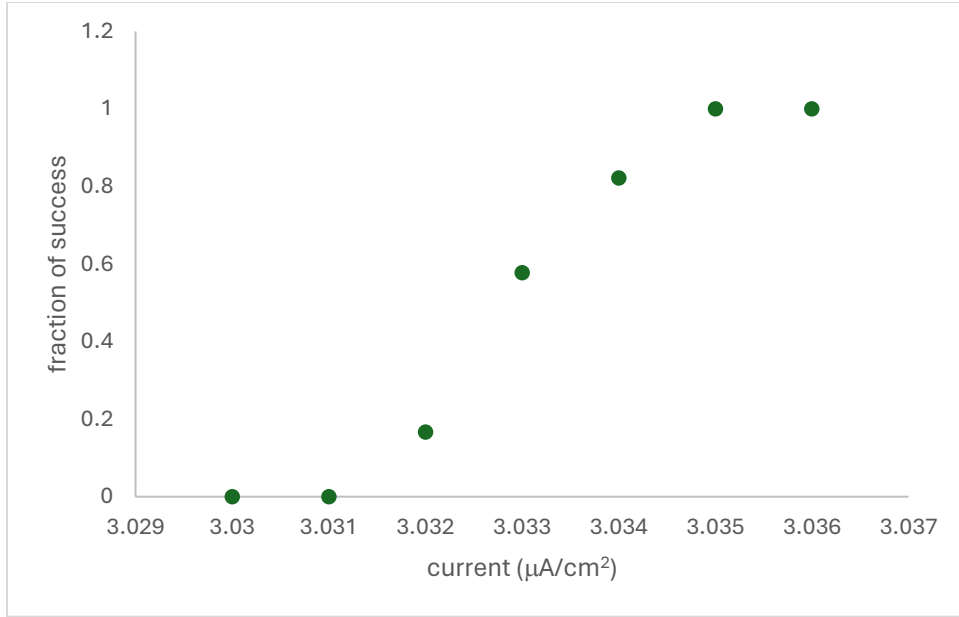


Figure 5.2. Success rate for single action potential firing for $\sigma = 0.005$

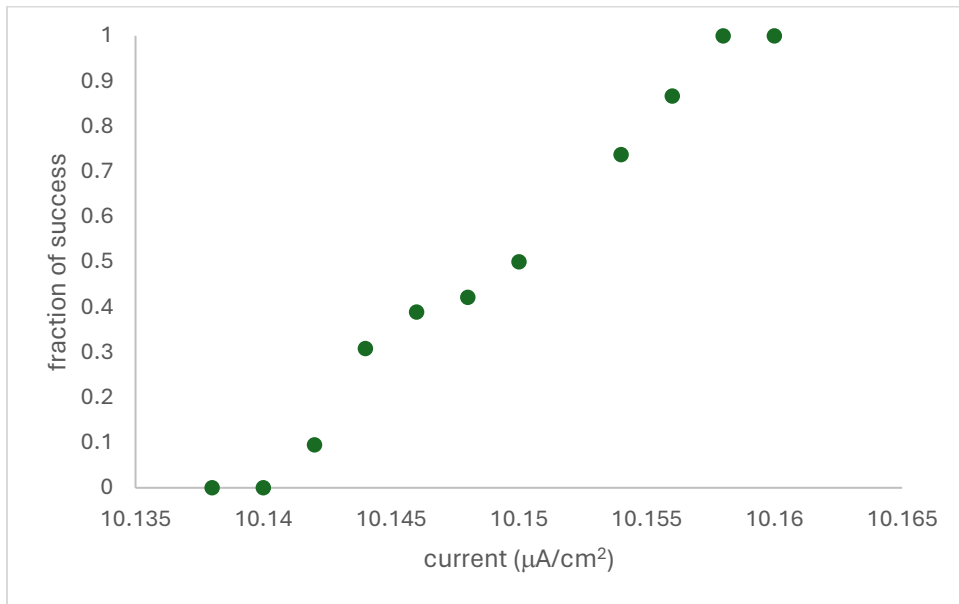


Figure 5.3. Success rate for single action potential firing for $\sigma = 0.05$

Thus, introducing a stochastic term as per the Euler-Maruyama method in the space-clamped HH equations had two main effects. Firstly, the current threshold for a single action potential was

greater than $2.24 \frac{\mu\text{A}}{\text{cm}^2}$. Secondly, there was a non-zero probability for below threshold currents to generate an action potential.

These results are just a preliminary sketch of how stochastic processes can be incorporated and interpreted in the Hodgkin Huxley model. Future work will focus on a more rigorous implementation of the theory of stochastic differential equations to this model. In particular, there has been relatively little work on incorporating stochastic terms in the full temporal-spatial equations; the vast majority of studies confine themselves to the space-clamped model.

Chapter VI: Conclusions

In this work we have demonstrated the essential features of the solutions to the Hodgkin Huxley model for neuron action potentials including all-or-nothing and refractory properties. In the full temporal-spatial solutions based on the cable equation, we have provided an initial interpretation in terms of a non-linear diffusion process. Finally, we have made some preliminary investigations into including stochastic effects in the model.

The Hodgkin Huxley model is a landmark achievement in the quantitative description of action potentials. Although other usually simpler models have also been proposed since their seminal work, the HH model continues to generate interest even after over 70 years, both as a fascinating problem in non-linear dynamics, as well as a robust model of actual processes occurring in neurons.

VII: Bibliography

- [1] B. Pakkenberg, H. J. Gundersen. Neocortical neuron number in humans: Effect of sex and age. *J Comp Neurol.* 1997;384:312-20
- [2] G. F. S. M. G. Cano (2016). Intermittency and Diffusion in the Hodgkin-Huxley Model. [Master's thesis, Técnico Lisboa].
- [3] Wanner, Mark. “600 Trillion Synapses and Alzheimers Disease.” *The Jackson Laboratory*, www.jax.org/news-and-insights/jax-blog/2018/december/600-trillion-synapses-and-alzheimers-disease. Accessed 20 Mar. 2024
- [4] R. Phillips, J. Kondev, J. Theriot and H. Garcia. *Physical biology of the cell*. Garland Science, 2012.
- [5] “APA Dictionary of Psychology.” *American Psychological Association*, 19 Apr. 2018, dictionary.apa.org/neuron. Accessed 12 Mar. 2024.
- [6] C. Henley, “Presynaptic Terminal.” *Foundations of Neuroscience*, Michigan State University Libraries, 1 Jan. 2021, openbooks.lib.msu.edu/neuroscience/chapter/the-neuron/. Accessed 18 Mar. 2024.
- [7] A. L. Hodgkin and A. F. Huxley. A quantitative description of membrane current and its application to conduction and excitation in nerve. *The Journal of physiology*, 117(4):500, 1952.
- [8] G. B. Ermentrout and D. H. Terman. *Mathematical foundations of neuroscience*. Springer, 2010.
- [9] M. Takebe, et al. “Mobilities and longitudinal diffusion coefficients for K⁺ ions in nitrogen and Argon.” *The Journal of Chemical Physics*, vol. 73, no. 8, 15 Oct. 1980, pp. 4071–4076, <https://doi.org/10.1063/1.440639>.

- [10] V. Palenskis. (2013, Feb. 27). Drift mobility, diffusion coefficient of randomly moving charge carriers in metals and other materials with degenerated electron gas. *SCIRP Open Access*.
https://www.scirp.org/html/13-4800160_28333.htm#return0
- [11] D. Johnston and S. M. Wu. *Foundations of Cellular Neurophysiology*, MIT, Cambridge, MA 1995
- [12] W. A. Catterall, et al. “The Hodgkin-Huxley Heritage: From Channels to Circuits.” *The Journal of neuroscience: the official journal of the Society for Neuroscience* vol. 32,41 (2012): 14064-73. doi:10.1523/JNEUROSCI.3403-12.2012
- [13] A. Iserles. *A First Course in the Numerical Analysis of Differential Equations*. 2nd ed. Cambridge: Cambridge University Press, 2008. Print. Cambridge Texts in Applied Mathematics.
- [14] D. Tan, Z. Chen. *On A General Formula of Fourth Order Runge-Kutta Method*”, *Journal of Mathematical Science & Mathematics Education* (2012)
- [15] J. B. Morton (1967). Numerical Solution of Hodgkin-Huxley’s Partial Differential System For Nerve Conduction. [Master’s thesis, Oregon State University].
- [16] Rieke, Fred. “Action Potential Propagation.” *Physiology*, 10 May 2023, uw.pressbooks.pub/physiology/chapter/action-potential-propagation/ (Modified from Lodish, *Molecular Cell Biology*). Accessed 18 Mar. 2024